

Wave in deck loads using Lagrangian Momentum Absorption (LMA) scheme

by

Koay Wen Xin

24495

Dissertation submitted in partial fulfilment

of the requirements for the

Bachelor of Engineering (Hons)

(Civil)

JANUARY 2021

Universiti Teknologi PETRONAS

Bandar Seri Iskandar

31750 Tronoh

Perak Darul Ridzuan

CERTIFICATION OF APPROVAL

Wave in deck loads using Lagrangian Momentum Absorption (LMA) scheme

by
Koay Wen Xin

24495

Dissertation submitted to the
Civil Engineering Programme
Universiti Teknologi PETRONAS
in partial fulfilment of the requirement for the
BACHELOR OF ENGINEERING (Hons)
(CIVIL)

Approved by,



(Dr. Mohamed Latheef)

UNIVERSITI TEKNOLOGI PETRONAS
TRONOH, PERAK

January 2021

CERTIFICATION OF ORIGINALITY

This is to certify that I am responsible for the work submitted in this project, that the original work is my own except as specified in the references and acknowledgements, and that the original work contained herein have not been undertaken or done by unspecified sources or person.



(KOAY WEN XIN)

ABSTRACT

When the water surface elevation exceeds the deck elevation and inundates the deck of fixed offshore structures, the resulting loads which are known as wave-in-deck loading leads to a step change in the loads acting on the structure. Given its importance, for predicting WID, a number of approaches exist, such as the well-known drag formulation and Kaplan's model. However, an important shortcoming of these models is the large number of empirical coefficients that ought to be obtained experimentally. A recently proposed model, known as Lagrangian Momentum Absorption (LMA) scheme overcomes these limitations by basing it upon the momentum dissipation that occurs during WID loading, removing the need for a large number of empirically tuned coefficients. This model can incorporate the details of the structure including its' porosity. This present work concerns the wave-in-deck load prediction on typical Malaysian jacket structures using local wave condition based on the newly proposed model. Given its' novelty, an implementation of this model is not available presently. Hence, the first stage of this project involved the development of computational code and verification of the developed code by comparing to existing upper bound solution. The second stage involved the computation of wave-in-deck loads for typical jacket structures in Malaysian conditions. The code that was developed in the present study has been validated by comparing to an existing momentum fluxbased model that provides a theoretical upper bound on WID loading. As expected, the developed code predicts close-to-zero forces for a fully permeable topside while close agreement was obtained for the case of a fully rigid deck. The wave-in-deck load was later computed using local wave condition on simplified topside where the wave properties were computed using linear wave theory. Generally, the wave-in-deck load was reduced when porosity is incorporated in the deck. Higher porosity within the deck results in lower wave-in-deck load. Similarly, the level of inundation was found to be an important contributor to the magnitude of the loads. Re-computing the loads using the nonlinear regular wave theory, Stokes' 5th order again showed that lower wave-in-deck load was predicted by LMA scheme. However, compared to the linear wave predictions, the nonlinear wave modelling led to a much higher force.

ACKNOWLEDGEMENT

First, I would like to extend my gratitude to my supervisor, Dr. Mohamed Latheef for his support along the way. He gave me an opportunity to do this great project topic. Dr Latheef devoted his precious time to teach and guide me, and always showing patience. He helped me in doing research and came to understand my work. I have learned and gained a lot of knowledge throughout the project. Without him, I would not be achieving so much as much as what I had today.

Besides, I would like to thank my understanding family especially my parent for their moral support and passionate encouragement in finishing this project within the limited time. They provided me a good comfortable and conducive learning environment which led me to the completion of this project successfully.

TABLE OF CONTENT

CERTIFICATION OF APPROVAL	i
CERTIFICATION OF ORIGINALITY	ii
ABSTRACT	iii
ACKNOWLEDGEMENT	iv
LIST OF FIGURES	v
LIST OF TABLES	vii
CHAPTER 1: INTRODUCTION	1
1.1 Background Study.....	1
1.2 Problem Statement.....	2
1.3 Objectives and Scope of Study	3
CHAPTER 2: LITERATURE REVIEW	4
CHAPTER 3: METHODOLOGY	13
CHAPTER 4: RESULTS AND DISCUSSION	17
4.1 MATLAB Code Computation... ..	17
4.2 Application of LMA Scheme on simplified topside structure using local wave condition.....	22
4.3 Stokes' 5 th order wave.....	32
CHAPTER 5: CONCLUSION AND RECCOMENDATION	37
REFERENCES	40
APPENDIX	43

LIST OF FIGURES

Figure 1.1.1:	Two offshore platform damaged during a hurricane off Louisiana... 2
Figure 2.1:	Horizontal WID loading process in three stages... .. 7
Figure 2.2:	Total WID loads of four different level of deck inundation based on LMA prediction compared to experimental WID loads... .. 10
Figure 2.3:	LMA load prediction and CFD results comparison based on four different level of deck inundation... .. 11
Figure 3.1:	Research methodology..... 13
Figure 3.2:	Momentum-intake module flowchart... .. 14
Figure 3.3:	Momentum dissipation module flowchart... .. 15
Figure 4.1.1.1:	Plan and elevation view for simplified topside for code verification 17
Figure 4.1.1.2:	Graaf’s model wave-in-deck force on front deck 18
Figure 4.1.1.3:	Graaf’s model wave-in-deck force on bottom deck..... 18
Figure 4.1.2.1:	Comparison of Graaf’s model and LMA scheme wave-in-deck load prediction on front (left) and bottom (right) deck when screen model of $P = 0.01$ 21
Figure 4.1.2.2:	Comparison of Graaf’s model and LMA scheme wave-in-deck load prediction on front (left) and bottom (right) deck when screen model of $P = 0.99$ 21
Figure 4.1.2.3:	Comparison of Graaf’s model and LMA scheme wave-in-deck load prediction on front (left) and bottom (right) deck when sponge model of $P = 0.01$ 22
Figure 4.1.2.4:	Comparison of Graaf’s model and LMA scheme wave-in-deck load prediction on front (left) and bottom (right) deck when sponge model of $P = 0.99$ 22
Figure 4.2.1:	Illustration of unmanned fixed offshore platform located at Sarawak, Malaysia (Mat Soom et. al., 2018)..... 23
Figure 4.2.2:	Plan view of simplified topside 24
Figure 4.2.3:	Elevation view of simplified topside 24
Figure 4.2.1.1:	Comparison of Graaf’s model and LMA scheme wave-in-deck load prediction on front (left) and bottom (right) deck when screen model of $P = 0.63$ when level of deck inundation at 0.4 m 25

Figure 4.2.1.2:	Comparison of Graaf's model and LMA scheme wave-in-deck load prediction on front (left) and bottom (right) deck when screen model of $P = 0.63$ when level of deck inundation at 0.7 m.....	26
Figure 4.2.1.3:	Comparison of Graaf's model and LMA scheme wave-in-deck load prediction on front (left) and bottom (right) deck when screen model of $P = 0.63$ when level of deck inundation at 0.9 m.....	26
Figure 4.2.1.4:	Comparison of Graaf's model and LMA scheme wave-in-deck load prediction on front (left) and bottom (right) deck when sponge model of $P = 0.63$ when level of deck inundation at 0.4 m.....	27
Figure 4.2.1.5:	Comparison of Graaf's model and LMA scheme wave-in-deck load prediction on front (left) and bottom (right) deck when sponge model of $P = 0.63$ when level of deck inundation at 0.4 m.....	27
Figure 4.2.1.6:	Comparison of Graaf's model and LMA scheme wave-in-deck load prediction on front (left) and bottom (right) deck when sponge model of $P = 0.63$ when level of deck inundation at 0.4 m.....	27
Figure 4.2.2.1:	Comparison of Graaf's model and LMA scheme wave-in-deck load prediction on front (left) and bottom (right) deck when screen model of $P = 0.3$ when level of deck inundation at 0.9 m.....	29
Figure 4.2.2.2:	Comparison of Graaf's model and LMA scheme wave-in-deck load prediction on front (left) and bottom (right) deck when screen model of $P = 0.4$ when level of deck inundation at 0.9 m.....	29
Figure 4.2.2.3:	Comparison of Graaf's model and LMA scheme wave-in-deck load prediction on front (left) and bottom (right) deck when screen model of $P = 0.63$ when level of deck inundation at 0.9 m.....	30
Figure 4.2.2.4:	Comparison of Graaf's model and LMA scheme wave-in-deck load prediction on front (left) and bottom (right) deck when sponge model of $P = 0.3$ when level of deck inundation at 0.9 m.....	30
Figure 4.2.2.5:	Comparison of Graaf's model and LMA scheme wave-in-deck load prediction on front (left) and bottom (right) deck when sponge model of $P = 0.4$ when level of deck inundation at 0.9 m.....	31
Figure 4.2.2.6:	Comparison of Graaf's model and LMA scheme wave-in-deck load prediction on front (left) and bottom (right) deck when sponge model of $P = 0.63$ when level of deck inundation at 0.9 m.....	31

Figure 4.3.1:	Surface wave elevation of Stokes' 5 th order wave.....	33
Figure 4.3.2:	Surface wave elevation of linear wave.....	33
Figure 4.3.3:	Stokes' 5 th order wave wave-in-deck load prediction on front (left) and bottom (right) deck when screen model of P = 0.63 under level of deck inundation at 0.4 m.....	34
Figure 4.3.4:	Linear wave wave-in-deck load prediction on front (left) and bottom (right) deck when screen model of P = 0.63 under level of deck inundation at 0.4 m.....	34
Figure 4.3.5:	Stokes' 5 th order wave wave-in-deck load prediction on front (left) and bottom (right) deck when sponge model of P = 0.63 under level of deck inundation at 0.4 m.....	35
Figure 4.3.6:	Stokes' 5 th order wave wave-in-deck load prediction on front (left) and bottom (right) deck when sponge model of P = 0.63 under level of deck inundation at 0.4 m.....	35

LIST OF TABLES

Table 4.2.1.1:	Percentage difference of total wave-in-deck load prediction for both screen and sponge model of P = 0.63 given different level of wave inundation... ..	28
Table 4.2.2.1:	Percentage difference of total wave-in-deck load prediction for both screen and sponge model of level of wave inundation at 0.9 m given different porosity of deck structure.....	32
Table 4.3.1:	Percentage difference of Stokes' 5 th order total wave-in-deck load prediction level of wave inundation at 0.4 m and P of 0.6... ..	36

CHAPTER 1

INTRODUCTION

1.1 Background Study

Oil and gas are currently the primary source of energy worldwide. Malaysia is petroleum producing country which remains the second largest petroleum producer in Southeast Asia, followed closely by Indonesia. Malaysia began oil exploration in 1970s, and until today, there are more than 250 installations have been operating for more than 20 years (Twomey, 2010). Nearly all of Malaysia's oil comes from offshore fields (U.S. Energy Information Administration, 2017) which are dotted around the relatively shallow Sunda shelf. In these relatively shallow water depths, the most commonly used structures to extract hydrocarbons are jacket platforms (Mat Soom et al., 2018). These jacket structures are subjected to different types of environmental loading of which the largest contribution comes from wave induced loads. For a jacket structure, wave induced loads can be further categorized substructure loads and wave-in-deck (WID) loads. Of these two, wave-in-deck loads is said to bring a significant impact load which governing the total wave load and thus performance of the offshore platform. It should be highlighted, due to the large magnitude, jacket structures are usually designed to avoid wave-in-deck loads by maintaining an effective airgap.

However, life expansion is often inevitable to optimize the usage of the platforms. These reassessments would usually require consideration of wave conditions that far exceed the design waves. This is exacerbated by the fact that sea bed subsidence may have reduced the design air gap considerably. In addition, for safety reasons, design standards always reduce the annual probabilities of exceedance for the design wave. It is typical to encounter 1 in 10,000 years (10^{-4}) for manned structures in harshest conditions.

Despite designing to avoid WID loads, evidence is mounting that WID loading occurs more often than expected. In fact, data obtained from Gulf of Mexico showed that more than 357 platforms (US Department of State, 2016; Hall, 2012) were destroyed

during Hurricane Katrina & Rita in 2005 and Gustave in 2008. More evidence can also be obtained from UK Health and Safety Executive (HSE) for WID loadings study on UK continental shelf. Figure 1 shows a typical example of damage caused by WID loads in Gulf in Mexico.



Figure 1.1.1. Two offshore platform damaged during a hurricane off Louisiana
(Kaiser and Chambers, 2017)

There are a number of existing models that are used for predicting WID loads. In fact, all of these existing models are currently adopted or recommended in most of the engineering design practice such as ISO (2014), API (2014), DNV-GL (2019b) and NORSAK (2017). However, most of these models utilize empirical loading coefficient on computation of WID loads. For any difference in the deck structure or wave conditions, these arrays of coefficients need to be tuned by fitting to more experimentally obtained design parameters which would be cumbersome and potentially expensive.

1.2 Problem Statement

The newly proposed WID loads computation model, called Lagrangian Momentum Absorption Scheme (LMA), that is based upon momentum dissipation is able to preclude the utilization of empirical inputs in describing wave in deck loads. It required no experimentally obtained parameter, and thus calibration of the formula. However,

this improved model is relatively new, and the MATLAB code of this scheme is not available yet. Besides, it hasn't been applied in the computation of wave-in-deck loads for any of the platforms South China Sea region.

1.3 Objectives

Given these two main issues mentioned, the objectives of the present study are:

- (i) To develop the MATLAB code for computation of WID load using Lagrangian Momentum Scheme (LMA).
- (ii) To apply the developed code to jacket deck in Malaysia using local wave condition.

Scope of study

This study will focus on computing WID load under regular unidirectional wave conditions.

CHAPTER 2

LITERATURE REVIEW

A few existing approaches have been introduced to describe the WID loads. It can broadly categorised into silhouette method or component-by-component approach. The former method assumes topside as a single rigid unit which the WID loads that act on the area of topside boundary is computed using simplest drag formulation. Equation (1) shows simplest drag formulation where the impact load is the heavily dependent on calibrated drag coefficient, C_{dd} .

$$F_{dd} = \frac{1}{2} \rho C_{dd} u^2 A \quad (1)$$

However, there is no detailed topside layout or components has been given attention when in fact, it reflects on how the topside responds on WID loads magnitude. This leads to the latter approach which topside layout or components based on different scenarios have to be considered separately.

The most used or widely known component-by-component approach is proposed by Kaplan et al. (1995) as suggested by engineering practices such as API (2014) and DNV-GL (2019b). This model predicts the WID loads acting on individual elements or large pieces of equipment. Based upon the drag formulation, WID loads is found by summation impact and drag load (Kaplan et al., 1995). Components that are adjacent to each other are defined as a single group and based on the flows of the wave particles in between these groups, velocity blockage effect will be considered. Empirical shielding factor will be introduced as well along the wave particles travelling distance. These give a reduced total WID loads acting on deck compared to drag formulation and thus provide a more accurate WID load prediction (Ma and Swan, 2020). Moreover, it is able to provide useful information on WID loads acting on each of the individual elements.

However, it is important to note that Kaplan's model heavily depends on different experimentally obtained design parameters such as empirical loading coefficient,

velocity blockage effects as well as shielding parameter. Recent study by Ma and Swan (2019) has observed that during impact loads, fluid is abruptly brought to rest, immediately after hitting the offshore structure with velocity being greatly reduced. This is the opposite of drag-type model presumed in Kaplan's model. This further emphasize on the dependence of velocity effect and empirical shielding factor in Kaplan's model, which would else produce WID loads prediction that are twice as large as the momentum flux formulation (HSE, 1998).

One of the examples given for the silhouette method is drag formulation, which in contrast, treats the entire deck as a single unit while computing WID loads. It formed part of Morrison's equation introduced by Morrison et al. (1950) which the WID loads prediction is based on calibrated empirical coefficient as well. While our interest falls on the surface waves, Ma and Swan (2020) mentioned that focus of Morrison's equation lies in force computation of fully submerged body where vicinity of surface wave is of a small part compared to submerged part which drag coefficient can be easily determined. Study showed that there are large uncertainties in obtaining coefficients even for less complicated case considered uni-directional waves on circular cylinder for surface waves, especially in steep near-breaking waves (Chaplin et al., 1992). Nevertheless, this model is widely used in engineering practice such as API (2014), ISO (2013) etc.

Having seen the limitation on utilizing empirical loading coefficient, a more preferred silhouette method would be the adoption of momentum flux formulation for calculation of WID loads. Graaf et al. (1995) first proposed this method to calculate the WID loads by transfer of wave momentum flux to deck boundary upon hitting the deck. This simple approach can be utilized when wave properties such as its surface elevation and velocity components that hit on deck is known.

Principle of momentum conservation is adopted which assumed all the momentum dissipation occurs instantaneously and is transferred to the deck as WID loads. It happens when the wave particles hit on the deck boundary, producing front and bottom deck WID load components. For a rectangular deck that allows wave particles to enter through underside, the total horizontal loads are then equated by summing these two force components as shown in Equation (2) and Equation (3) for below.

$$F_f(t) = \rho \overline{u^2} \phi_{ff} - h_{dd} \phi_{bb} \quad (2)$$

$$F_{bb}(t) = \rho g u b \quad (3)$$

Equation (2) and Equation (3) correspond to WID load on front deck and bottom deck respectively, which horizontal velocity u , vertical velocity v , surface elevation η , wave density ρ , height of deck h_d , and width of deck b . Ma and Swan (2019) have carried out an experiment to study the different waves properties and its effects on WID loadings behavior based on the momentum flux formulation. This study has covered the occurrence of different types of wave and their crest behaviors with the possibility of beyond second order, which provides a more realistic insight of WID loadings on offshore structures. This is different from common design practice of analyzing waves using regular wave theory. In this experiment, a topside of 60 x 60 m has been constructed with a model length scale of 1:100 (0.6 x 0.6 m). A variety of deterministic waves have been selected based on realistic JONSWAP spectrum. In each case, different wave properties were allowed to alter and WID load was measured. Based on this experiment, a physical explanation on WID loading on wide range of wave forms has been obtained.

In describing these wave forms, the simplest is given by a linear regular wave, of which, the surface elevation is given by the simple sinusoidal function,

$$\eta = \alpha \cos(\omega t - k d) \quad (4)$$

where α , ω ($2\pi/T$) and k ($2\pi/\lambda$) are wave amplitude, wave frequency and wave number respectively. The wave kinematics associated with this linear wave is given by

$$u = \frac{\alpha \omega \cosh(k(y+d))}{\sinh(kd)} \sin(\omega t - k d) \quad (5)$$

$$v = \frac{\alpha \omega \cosh(k(y+d))}{\sinh(kd)} \cos(\omega t - k d) \quad (6)$$

where Equation (5) and Equation (6) correspond to horizontal and vertical wave kinematics respectively and d is the water depth from still water level. For a regular wave, once nonlinearity is incorporated, additional terms are required in the solution and the most commonly adopted solution is the Stokes' 5th order solution (Fenton, 1985) which gives the surface elevation as

$$\eta = \sum_{i=1}^5 B_i \cos(\omega_i t - k_i d) \quad (7)$$

where B is the function of water depth d and wave number k. And wave kinematics u and v given by

$$u = C_0 \sum_{i=1}^5 \left(\frac{g}{k} \right)^{1/2} \sum_{j=1}^i A_{ij} \cos(k_j(z+d)) \cos(k_i d - \omega_i t) \quad (8)$$

$$v = C_0 \sum_{i=1}^5 \left(\frac{g}{k} \right)^{1/2} \sum_{j=1}^i A_{ij} \sin(k_j(z+d)) \sin(k_i d - \omega_i t) \quad (9)$$

where C₀ and A_{ij} are again functions of water depth d and wave number k.

A typical WID loading process with respect to time is presented by Ma and Swan (2019) from the experiment. Focus has been given on horizontal component of WID loading as it contributed most to the offshore structural failure, rather than relatively small vertical loadings associated with small vertical velocity at crest (Graaf et. al., 1995). Figure 2.1 below shows the three different stages of WID loadings with its incident wave profile.

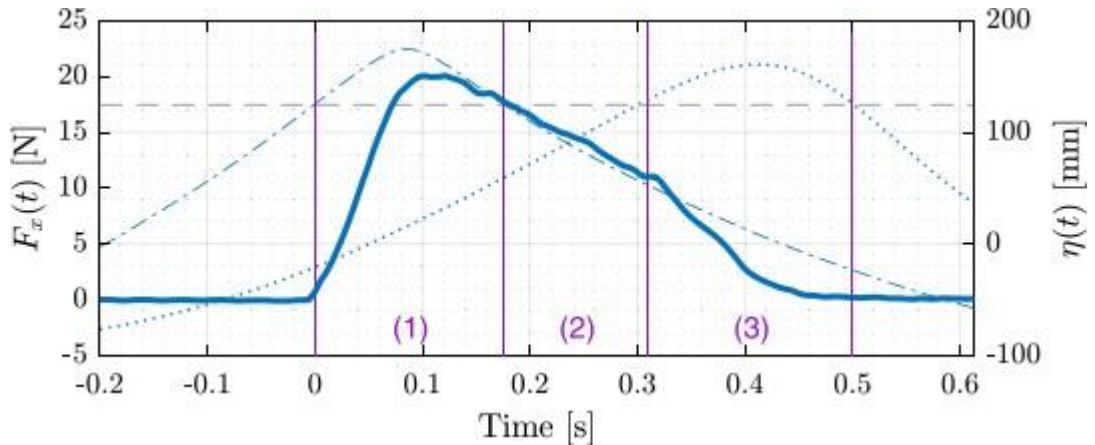


Figure 2.1. Horizontal WID loading process in three stages, [—] total measured horizontal WID loads, [---] wave surface elevation at front face of deck, [···] wave surface elevation at bottom face of deck, [---] the deck underside elevation (Ma and Swan, 2019).

Based on Ma and Swan (2019), the three stages of WID loadings process are as below:

- (i) Wave entry when the level of deck inundation is higher than that of height of deck. It is this time that the waves enter the topside structures and hit the front and bottom of deck. Along with increasing wave kinematics and wave crest of incoming waves, there will be sharp rise in WID loads until the maximum WID loads occurs. This stage ends with wave inundation level finally lower than that of height of deck where it happens after a decreasing WID loads followed by waves leaving the front face.
- (ii) Upon waves leaving the front deck, waves are allowed to enter only through underside. At this stage, the waves propagate along the bottom of the deck. The associated mass flow rate and wave kinetics reduced leading to a decrease of WID loads. This stage ends with wave profile reach the backside of deck.
- (iii) At the third stage, there is only a little water enters the topside structure when wave profile leaving the topside. As a result, WID loads falls back to zero almost immediately. The loading cycle ends with wave profile completely leaves the topside.

Based on the given relationship between the WID force and associated wave profile, Ma and Swan (2019) have presented the WID loads obtained from different deterministic wave cases. This is achieved by consideration on different spectral peak period, directional spread and spectral bandwidth while kept other parameter constant on each case. Generally, all the cases followed the typical shape of wave loading stage as shown in Figure 2.1 above, but with different amplification of magnitudes of WID forces. Some normalizations have been done to find the influence of two variables: wave shape and wave kinematics. From this experiment, it is known that wave shape acts as dominant or monitoring factor on WID loads, followed by wave kinematics. However, both are undoubtedly contributed to momentum rate transferred from waves to the deck (Ma and Swan, 2019).

However, Graaf et al. (1995) proposed model used in this experiment treats topsides as a single unit and for waves that hit the deck boundary are assumed to have dissipated immediately and are transferred to deck as WID load. It is noted that no porosity in topside layout is being considered for this model. In this case, any remaining

momentum that passes through these porosities is not computed. As a result, this model gives an upper boundary solution (Ma and Swan, 2020). While WID loadings are commonly associated with largest waves in severe sea states (Graaf et al., 1995), such waves will experience effect of second order or above and wave breaking, even in intermediate and deep-water depth (Latheef and Swan, 2013). As it can be seen from Equation (2) and Equation (3) that computation of WID loads is governed by both wave shape and water particle kinematic (Ma and Swan, 2019), full understanding of wave characteristic is required. This raised the concern of whether the abovementioned model is able to accurately describe the wave characteristic and provides accurate WID load projection.

Ma and Swan (2020) have proposed an improved model of WID loads computation by utilizing momentum flux formulation introduced by Graaf et al (1995). This improved model has adopted an approach which progressive dissipation of wave momentum is considered when wave hits the topside layouts. Upon reaching the deck boundary, individual wave particles are tracked and different rate of momentum loss is encountered when these particles travelled within the topside and hit on different topside features. These different rates of momentum dissipated is depending on porosity associated with topside features. Incoming wave particles are grouped as 'momentum parcel' (MP) based on time instant and their position is tracked within the deck. The summation of all these different rates of momentum flux will then give the WID loads. It is noted that along the WID load computation process, no empirical loading coefficient has been involved.

Ma and Swan (2020) has done some comparison to prove the viability of LMA scheme in WID load prediction. First is the comparison between LMA scheme and laboratory experimental results on WID loads. The wave conditions are reproduced as of the laboratory experiment and the WID loads found is shown in the Figure 2.2 below. Figure 2.2 below shows the WID loads on particular cases involved four different level of deck inundation while keeping all other wave parameters constant for each variation. It can be seen that the LMA scheme is able to predict WID loads quite similar to the experimental measurement.

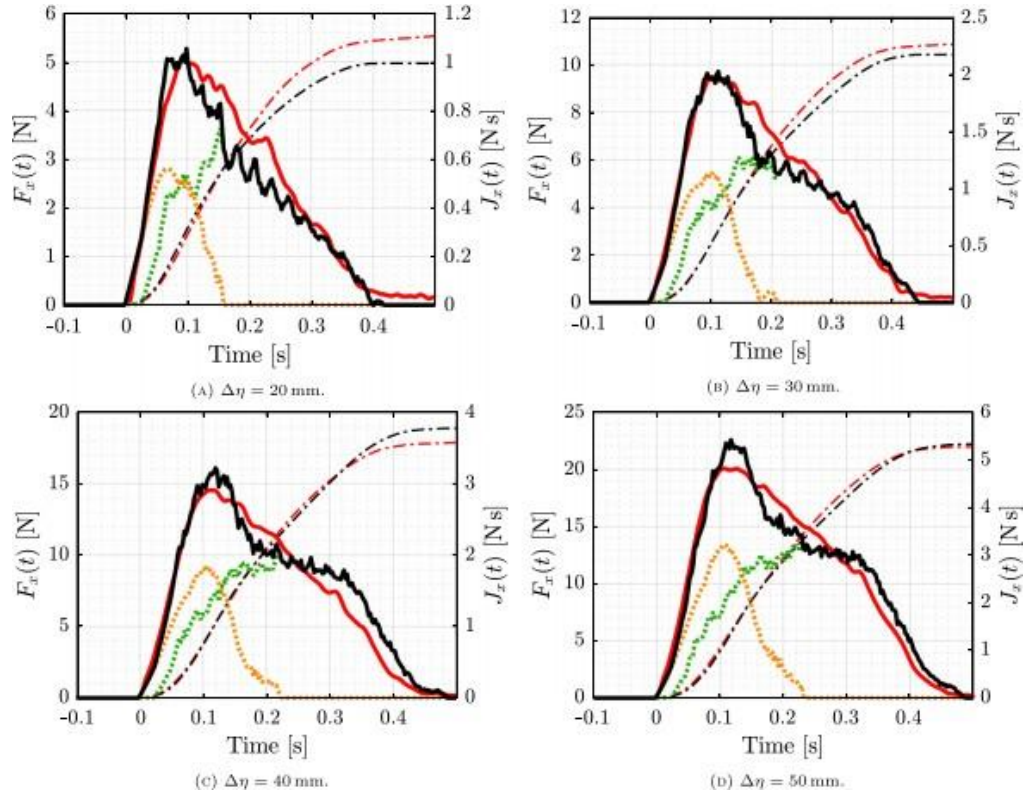


Figure 2.2. Total WID loads of four different level of deck inundation for $P = 0.63$ and $h_d = 125$ mm. Wave cases taken is based on focused wave in uni-directional JONSWAP spectra with $\gamma = 2.5$ and $T_p = 1.6$ s. Each sub- figure includes [—] total measured WID loads based on LMA prediction which is the sum of [····] WID load at front face of deck, [····] WID load at bottom face of deck, [-·-·] predicted momentum compared to [—] experimental WID loads and [-·-·] experimental momentum (Ma and Swan, 2020).

Besides, Ma and Swan (2020) have compared on WID loads computation between LMA scheme and computational fluid dynamics (CFD) as well. Similar to previous comparison, while keeping all the wave parameters constant, the variation of each of this comparison is only on four different level of deck inundation. The resultant WID loads is given as Figure 2.3 shown below. A good agreement between two WID loads prediction can be seen from the Figure 2.3. Based on the two mentioned comparison, it can be said that LMA scheme is able to produce a satisfying result on load prediction, even without the usage of empirical loading coefficient while considering non-instantaneous dissipation of momentum.

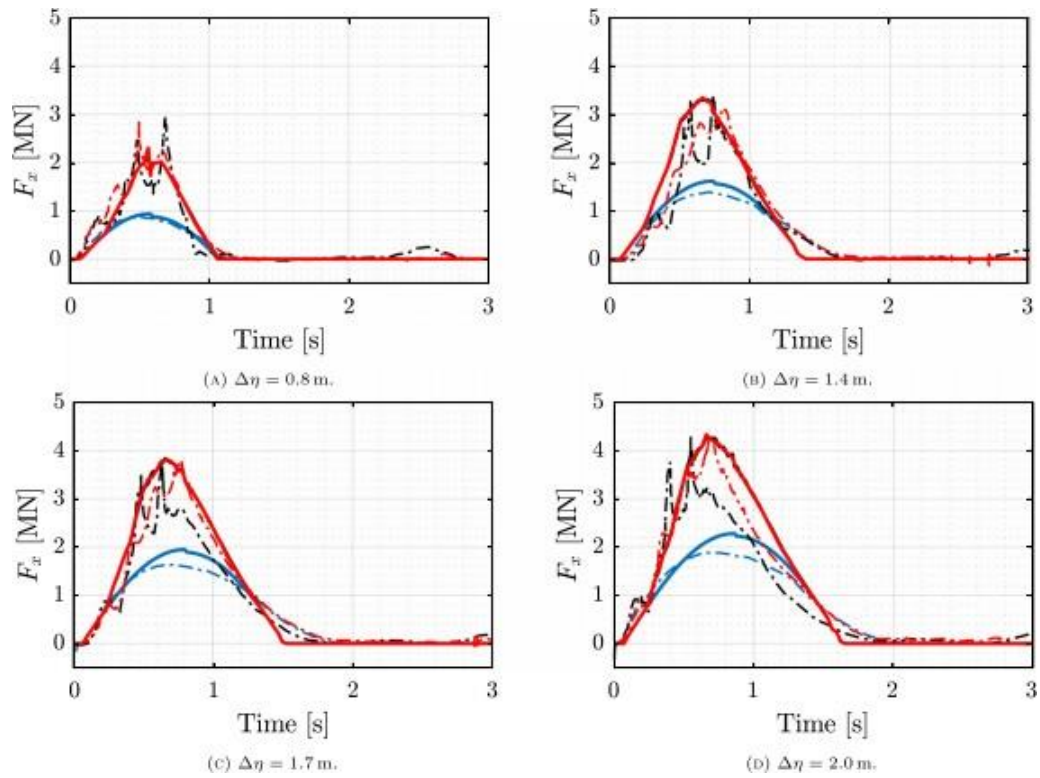


Figure 2.3. LMA load prediction and CFD results (Chen et al, 2018) comparison based on four different level of deck inundation. For topside condition 1: — LMA prediction and - - - CFD results for topside condition 2: — LMA prediction and - - - CFD results, for topside condition 3, — LMA prediction and - - - CFD results for each sub-plot (Ma and Swan, 2020).

LMA scheme is able to cater the non-instantaneous dissipation of wave momentum while incorporate with porous topside structure. As Ma and Swan (2020) stated, there are two modules involved in this model, first is the momentum intake module and second is the momentum dissipation module. This model enables the tracking of the momentum parcel within the deck and gives a different rate of momentum dissipations. The good thing about this LMA scheme is that no empirical loading coefficient has been used and each of this module is actually independent of each other and thus multiple time of execution can be supported. As proposed by Ma and Swan (2020), two modules were applied accordingly and will be executed as sequentially. More detailed of execution will be discussed in latter section. It is noted that there will be no empirical loading coefficient used while considering different rate of momentum dissipation.

Ma and Swan (2020) mentioned that LMA scheme is indeed able to give a relatively simple but good prediction on WID loading provided a wave event is properly captured. It is noted that no empirically determined coefficient has been included. In fact, two modules introduced herein can be utilize independently, with different topside internal layout on a constant wave condition or vice versa. The flexibility given by LMA scheme is able to compute full probabilistic analysis of WID loadings on severe sea state especially when designing or reassessment of offshore structure is required.

CHAPTER 3

METHODOLOGY

The methodology of this study is shown as Figure 3.1 below.

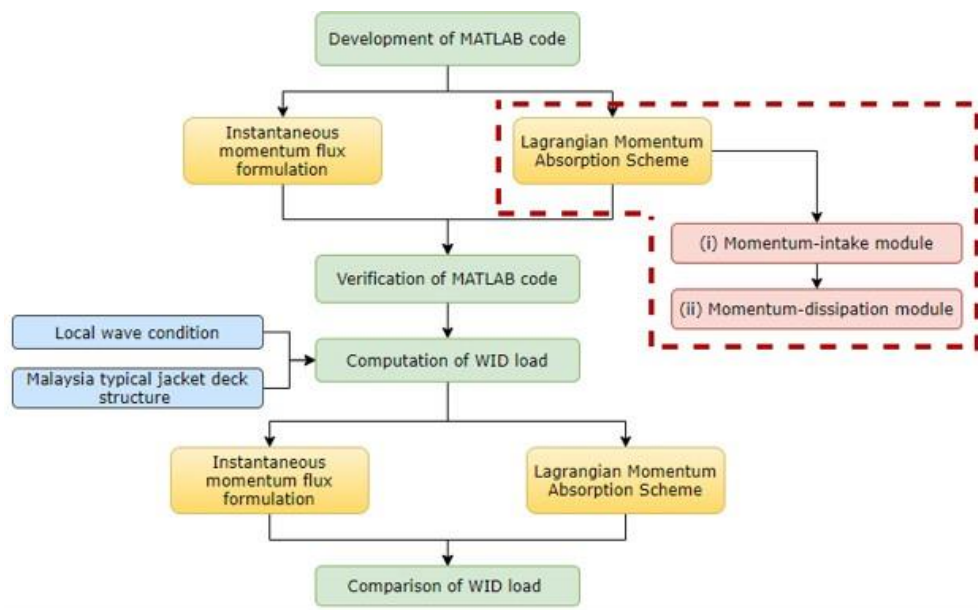


Figure 3.1. Research methodology

Code generation for existing model of momentum flux formulation will first implemented. WID loads will then computed based on principle of momentum conservation. Code for improved model of LMA scheme will then developed which two modules will be involved which is momentum-intake module and momentum dissipation module. These two modules will be discussed further under same section later on. The code verification for both of the model will be done by manuals calculations or comparing the analytical values generated from different formulas. The codes will be refined if any errors were found and the first objective is thus achieved as this stage. The parameters of local wave properties and typical jacket structures will be obtained from PTS for WID loads computation purpose. These data will be fitted in to both of the existing model and improved model to finally compare both of the results. A detailed procedure on application of two modules will be as below

(i) Momentum intake module

This module aims to find out the initial wave profile and wave kinematics, and thus initial momentum upon hitting the boundary of structure topside. The momentum intake module will first be executed by defining the deck boundary into horizontal and vertical panels, each receives initial horizontal (u^2) and vertical velocity (uv) respectively. These panels will then further discretize into small elements, k . For each of this element, the wave kinematics (ρu^2 or ρuv) on each element node will be computed. This value is then integrated with the area of element to get the rate of the momentum $(\frac{dJ}{dt})_{i,k}$ and finally the momentum can be found by the product of rate of momentum with difference in time instant (

$J_{i,k} = \int_{i,k} \frac{dJ}{dt} \Delta t$). The process will be repeated for each of the small elements within the same time instant and for the next time instant. The wave momentum that arrived at the deck boundary element within the same time instant is called a momentum parcel (MP). The flow chart for momentum intake module execution is as shown below.

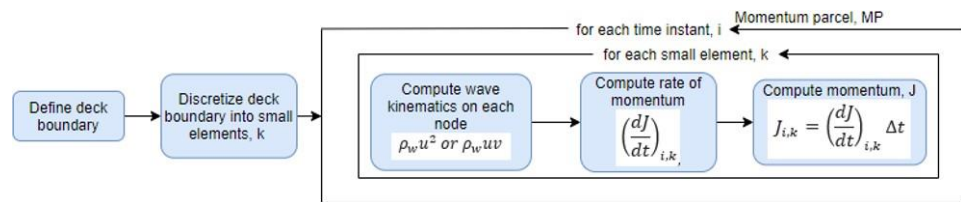


Figure 3.2. Momentum-intake module flowchart, adopted from Ma and Swan (2020)

(ii) Momentum dissipation module

This module concerns with the displacement (x) of each MP with a known topside internal layout. The initial momentum output obtained from previous module will then be fit into this module. During this time, there will be a number of MPs within the deck, either from previous or new time instant. For each MP, the displacement and new location ($x = u \Delta t$) will be defined. Calculations for any MP that lies outside of deck boundary upon reaching new location is precluded. Based on their trajectory, their location is tracked if they encounter any topside features, if yes, there will be momentum dissipation occurs and the remaining momentum will be

calculated. New velocity associated with remaining momentum will then be adjusted for next time instant on each MP. The adjusted velocity is based on the loss of the momentum of each MP due different porosity defined on topside features. This process will be repeated for each of the MP within the same time instant. The summation of the rate of change of momentum for all these MPs will gives the WID loads ($F_{dd}(t) = \sum \frac{\Delta J_m}{\Delta t}$) for that particular time instant. This process will then be repeated for next time instant until all of the MPs final leaves the deck. The flow chart for momentum dissipation module execution is as shown below.

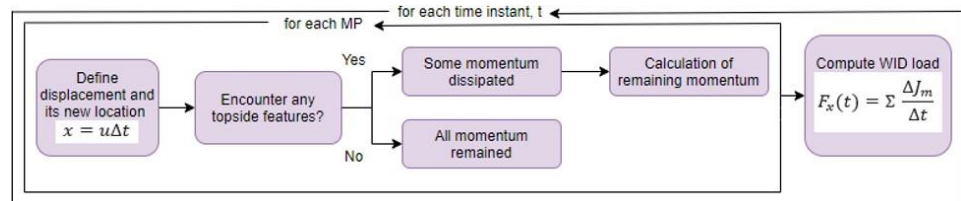


Figure 3.3. Momentum dissipation module flowchart, adopted from Ma and Swan (2020)

Porosity of topside features needs to properly defined to capture the progressively loss of momentum flux. Ma and Swan (2020) have proposed two approaches of modelling porosity of topside features. A ‘screen’ or sequence of ‘screen’ is used to represent a relatively compact plan area or discrete features. In this case, each ‘screen’ was taking a proportional of openness of P , and thus the loss of momentum is reduced and has a factor of $(1-P)$ of initial momentum J_0 when first ‘screen’ is encountered and so on. Upon leaving the topside, there were some remaining momentum of MPs and the associated dissipated momentum. After passing through n number of screens, the remaining momentum will be equal to Equation (10) below.

$$J_n = J_0 P^n \quad (10)$$

where $J_n \geq 0$. In contrast, continuous features that occupied a large volume are represented by a ‘sponge’ component. For this case, the momentum loss is depending on the path (X) taken by MPs along the ‘sponge’ over a change in time instant. This approach precludes any projection happens outside the sponge defined. The remaining momentum J_i identified as an exponential decay formulation as shown in Equation (11) below.

$$I_i = I_{i-1} e^{\beta P \Delta x_i} \quad (11)$$

where decay constant, $\beta = \frac{\ln PP}{\Delta \Delta}$. Both of these approaches can be used to model different porosity of topside features, provide flexibility in both spatial and direction variables (Ma and Swan, 2020). Accurate load prediction can be produced if the correct approach of porosity definition is modelled.

Upon the determination of new location and associated remaining momentum of MPs, velocity adjustment is required. Momentum is obtained by multiplying mass and velocity. Thus, a reduced in remaining momentum within the deck is either attributed to reduced velocity or mass. Ma and Swan (2020) have mentioned that for a topside feature with large porosity ($P \rightarrow 1$), the momentum loss is mainly attributed to reduced velocity and correspond to lower-bound. In contrast, a reduction of momentum can be associated with dominant effect of mass blockage when the porosity is small ($P \rightarrow 0$) and correspond to upper-bound. However, these adjusted velocities are simply used to give the position of MPs and does not involved in WID loads calculation. The adjusted velocity for remaining momentum will be given as Equation (12) below:

$$u_i = [1 - kPP(1 - r)] u_{if} \quad (12)$$

CHAPTER 4

RESULTS AND DISCUSSION

4.1 MATLAB Code Computation

4.1.1 Van de Graaf's Model

Code generation for Graaf's model on wave-in-deck loads computation is first implemented as discussed in Chapter 3. The code developed is such that the momentum is dissipated instantaneously upon hitting the deck boundary, as indicated by Graaf's model. A 20 m x 15 m deck, with a height of deck of 0.5 m located at the water depth of 60 m is adopted with a level of wave inundation at approximately 0.5 m.

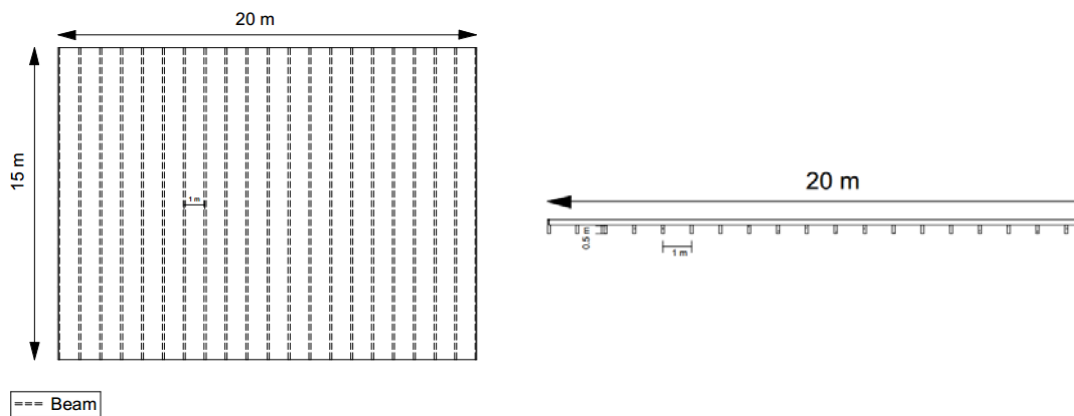


Figure 4.1.1.1. Plan and elevation view for simplified topside for code verification

Figure 4.1.1.2 and Figure 4.1.1.3 show the wave-in-deck load-time history for front deck and bottom deck respectively. Figure 4.1.1.2 shows an increase in force magnitude upon wave entry. It reaches the peak force magnitude when the level of wave inundation is at the highest. The wave then leaves the front deck as it propagates which leads to a decrease in force magnitude and finally reaches zero force magnitude when all the wave particles leave the front deck. Figure 4.1.1.3 shows a force

increment when the wave starts enter the bottom deck boundary. It comes to a peak and remain constant for the amount of time when maximum number of wave particles is able to reach the boundary. It is followed by a decrease in force magnitude when wave reaches and leaves the end of deck. Both Figure 4.1.1.2 and Figure 4.1.1.3 depict the expected typical WID loading pattern as shown in Figure 2.1 which the summation of forces acting on both front and bottom deck will give the total WID load.

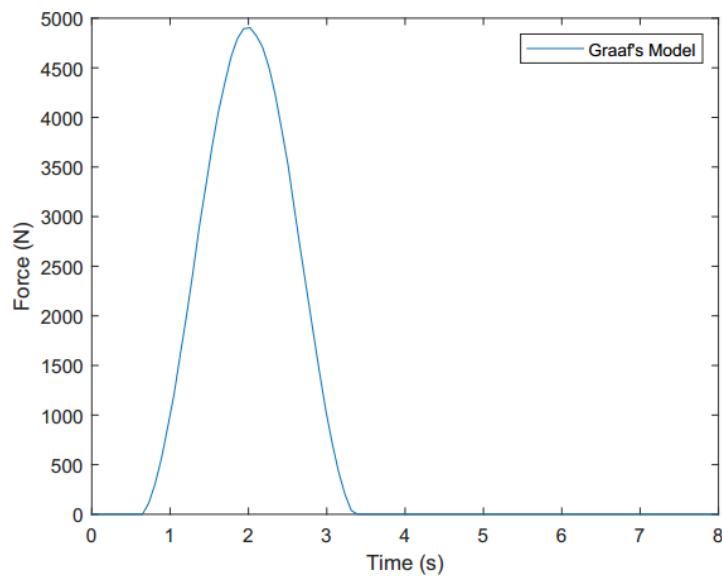


Figure 4.1.1.2. Graaf's model wave-in-deck force on front deck

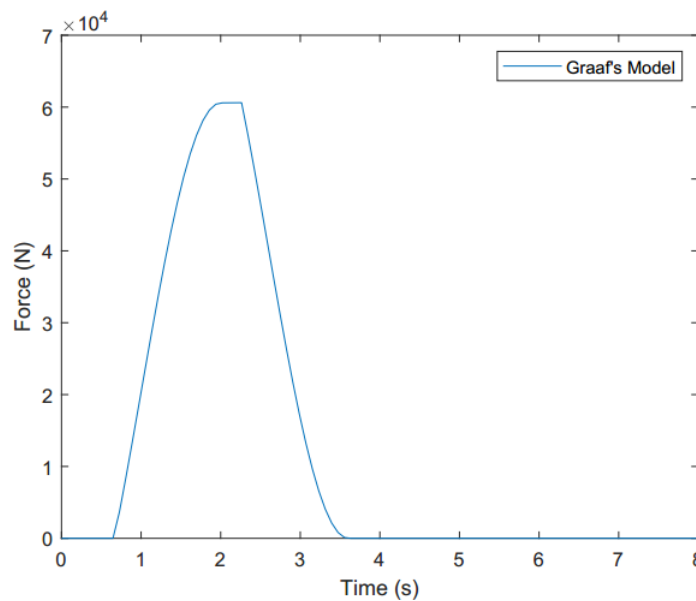


Figure 4.1.1.3. Graaf's model wave-in-deck force on bottom deck

As there is no available wave data on Graaf's existing results, the code is validated by manual calculation attached in Appendix and with that it is confirmed that the code is able to generate a correct WID load prediction. It is important to ensure the code developed in this stage is correct as the generated results will act as a baseline for comparison and code verification in LMA scheme in further section such that it provides an upper bound WID load prediction.

4.1.2 Lagrangian Momentum Absorption Scheme

Momentum intake module

This module serves as the input for next module. In fact, the code developed for this module is derived from Graaf's model code, with added information on initial position of each wave particle that reaches the deck boundary with their respective wave kinematics. In this stage, the summation of all the wave kinematics within the same period give the same load prediction as in Graaf's model, given the same wave data have been inputted.

Momentum dissipation module

Porosity (P) in deck is introduced in this module, either by screen or sponge model depending on the internal features of the deck. The code is developed in such a way that users are free to input the number of walls within the deck and its associated porosity. Based on Ma and Swan (2020) research, lower total WID force as compared to Graaf's model will be expected if the deck is porous, which will be used to validate the applicability of the code.

(i) Screen model

Equation (10) is utilized to incorporate the porosity into the computation of WID force. In this model, the code developed allows the porosity (P) of each wall to be different, as suggested by Ma and Swan (2020).

(ii) Sponge model

Equation (11) is used to describe the WID force by associating it with the displacement taken by each MP. As oppose to screen model, Ma and Swan (2020) formulate the WID force by assuming the porosity (P) is averaged out of the deck as a whole component.

Based on the formulation of finding the remaining momentum, both equations suggested that the higher the value of P (when compared between same number of walls), the more the remaining momentum left upon leaving the deck. This leads to the expectation of lower total WID load prediction. In contrast, the more the number of walls (when value of P kept constant for all walls), the less the remaining momentum left upon leaving the deck.

Besides, the code is developed such that the velocity adjustment will be executed every time an MP passed through a wall to take account of the effect of either mass blockage or reduced velocity, depending on value of P . Thus, it brings the total WID load lesser, but not significant, as the primary purpose for this step is to find the displacement of each MP.

Unfortunately, there is no available wave data on existing results (Ma and Swan, 2020) for validation purpose. Thus, two simplified cases were run for each model for code verification purpose. The first case is simply setting P near 0. This case represents a deck with almost zero or no porosity within the deck which is similar to the assumption made by Graaf's model. As a result, maximum total WID force will be anticipated as momentum is considered dissipated instantaneously upon hitting the first wall, which should be close to the upper bound load prediction obtained in Graaf's model.

As oppose to the first case, second case is to set the P near 1, which assumed equivalent to almost no blockage exists in the deck. This means that all the MPs are allow to enter and leave the deck freely without any momentum dissipated. The outcome is expected to be the minimum WID force or near zero WID force. For both cases, the same wave data and deck size would be adopted.

To achieve this, porosity (P) of 0.01 and 0.99 will be taken for first and second case respectively on two LMA models. Also, a 20m x 15m deck is adopted with a level of wave inundation at approximately 0.5m for both load prediction approaches. Figure 4.1.2.1 and Figure 4.1.2.3 shows the WID load-time history of Graaf's model and LMA scheme when both screen and sponge model of $P = 0.01$ for front deck and bottom deck respectively. The comparison between two approaches suggested that the code developed for both models is able to produce an expected LMA load prediction which is close to upper bound WID load when P is near 1. This is due to none of the MP has remaining momentum left upon hitting the first wall within the deck as no

porosity will be available for MPs to pass through and no velocity adjustment will be executed. Figure 4.1.2.2 and Figure 4.1.2.4 shows the WID load-time history of Graaf's model and LMA scheme when screen and sponge model of $P = 0.99$ for front deck and bottom deck respectively. A huge WID load prediction difference between the LMA scheme and Graaf's model is observed. In fact, a supposed close to zero WID load for LMA scheme is found as no MPs hit the deck's wall when it propagates freely along the deck in both models.

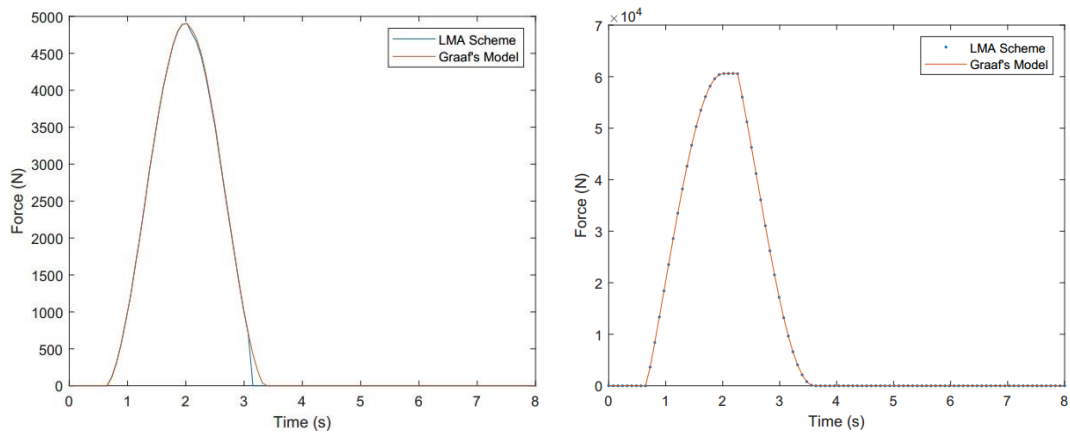


Figure 4.1.2.1. Comparison of Graaf's model and LMA scheme wave-in-deck load prediction on front (left) and bottom (right) deck when screen model of $P = 0.01$

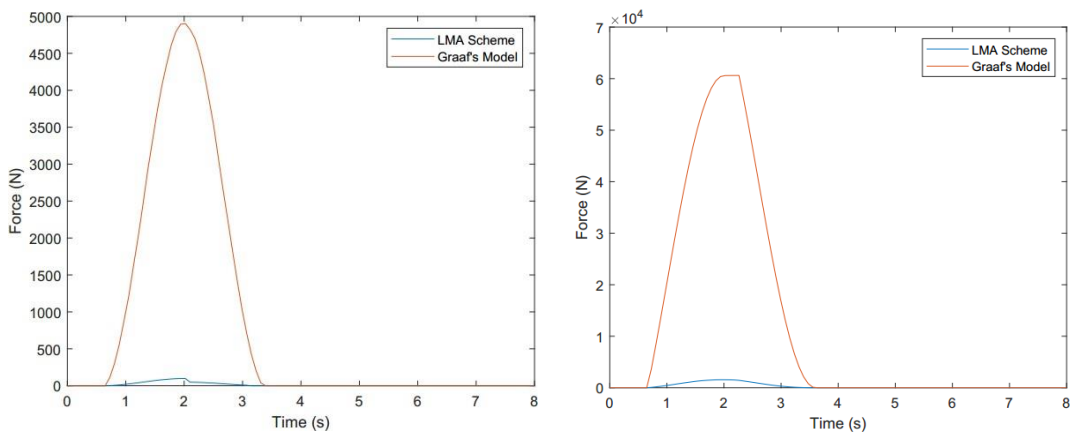


Figure 4.1.2.2. Comparison of Graaf's model and LMA scheme wave-in-deck load prediction on front (left) and bottom (right) deck when screen model of $P = 0.99$

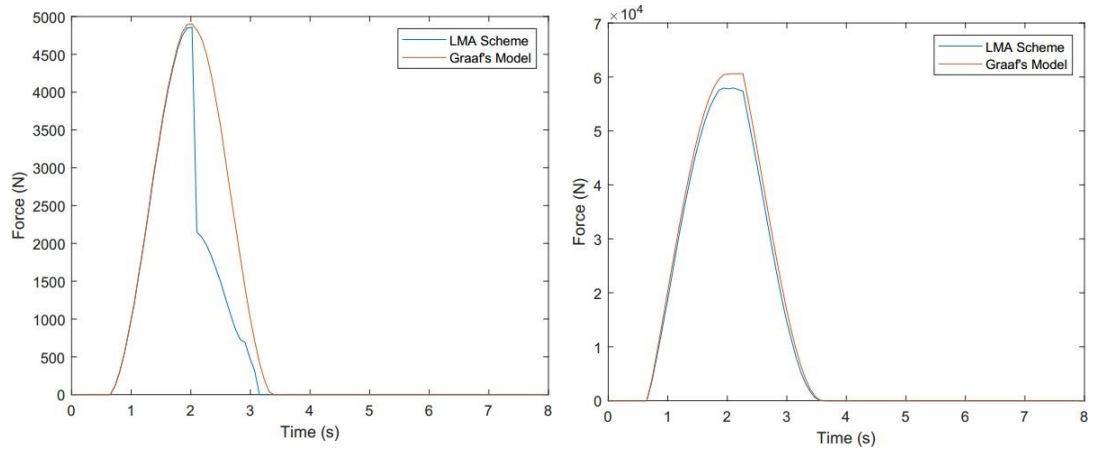


Figure 4.1.2.3. Comparison of Graaf's model and LMA scheme wave-in-deck load prediction on front (left) and bottom (right) deck when sponge model of $P = 0.01$

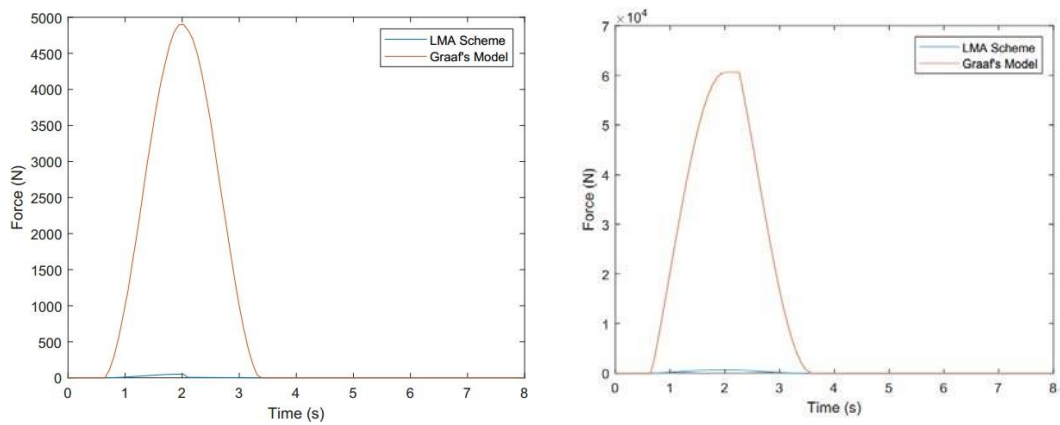


Figure 4.1.2.4. Comparison of Graaf's model and LMA scheme wave-in-deck load prediction on front (left) and bottom (right) deck when sponge model of $P = 0.99$

Figure 4.1.2.1, Figure 4.1.2.2, Figure 4.1.2.3 and Figure 4.1.2.4 suggested that the code developed is indeed able to reproduce the intended LMA load prediction. Besides, it should be recalled that while the code produced is able to support different topside porosities inputs, no empirical coefficient inputs are required to generate the WID load prediction, as suggested by Ma and Swan (2020).

4.2 Application of LMA Scheme on simplified topside structure using local wave condition

Given the novelty of LMA, to the author's knowledge, none of the South China Sea region has used LMA scheme for WID load prediction. Therefore, the MATLAB code

of LMA scheme presented is utilized for WID load computation on a simplified deck structure found in Malaysia using local wave condition to provide better accuracy of WID load. With this, a realistic deck structure can be represented when WID load is calculated as its associated porosity is taken into account. This is important as the effect of WID load prediction due to topside porosity is justified. To study this, a comparison between Graaf's and LMA scheme WID load prediction of a simplified topside structure with varied wave and topside properties, particularly level of wave inundation and topside porosity are carried out.

Topside structure configuration

A simplified topside with reference to an unmanned deck structure located at Sarawak, Malaysia shown in Figure 4.2.1 is modelled with an overall geometry of 30 m x 12 m. Overall deck thickness of 1.035m including the plate with underside beams of 1m deep span across the deck width are modelled all across the topside with 1m apart between each other for all of the cases. The deck flooring is modelled to allow for wave to enter from the bottom of the deck and so the WID load contributed by the wave hitting the bottom deck will be observed as well. Figure 4.2.2 and Figure 4.2.3 show the plan and elevation view of the simplified topside Details on the associated porosity for each case will be mentioned in their respective results. It should be noted that, the layout of the beams and their depths are assumed and in practice expected to be more widely spaced and potentially smaller in size. However, for this preliminary calculation, it was assumed that this would suffice.

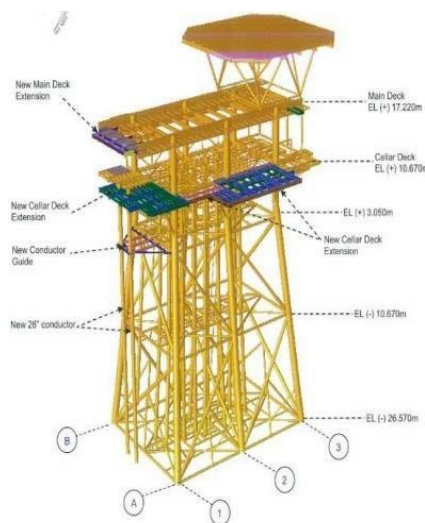


Figure 4.2.1. Illustration of unmanned fixed offshore platform located at Sarawak, Malaysia (Mat Soom et. al., 2018)

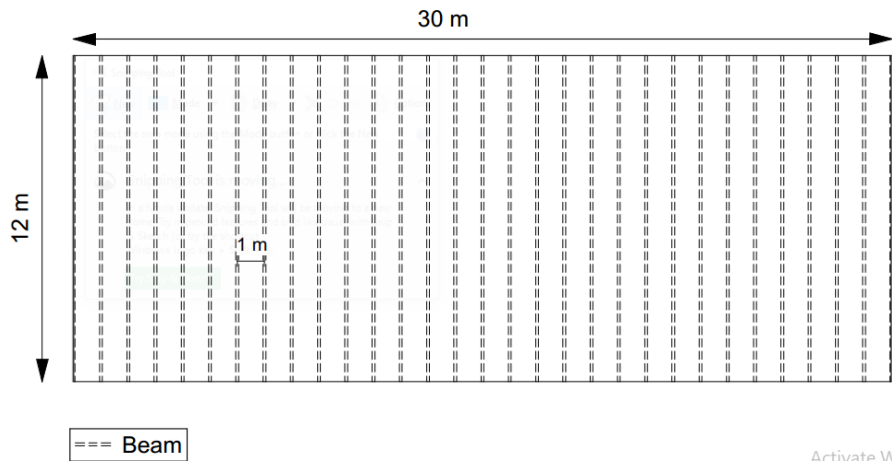


Figure 4.2.2. Plan view of simplified topside

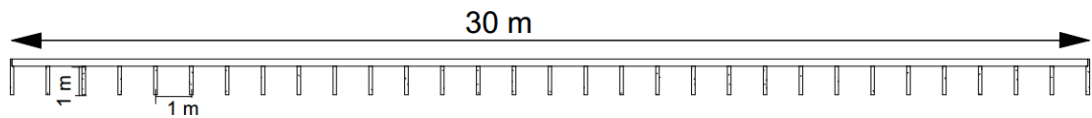


Figure 4.2.3. Elevation view of simplified topside

Wave properties

The WID load prediction is computed based on the local wave condition with water depth of 65 m. A wave period of 10 s with a wave height of 12 m is modelled. This roughly relates to 100-year storm conditions in Peninsular Malaysia. These wave properties represent the waves that will be propagated along the topside and are kept constant for all of the cases. However, the level of wave inundation will be a function of height of the topside structure instead of wave height. Details on the level of wave inundation will be given in their respective results.

4.2.1 Variation on level of wave inundation

The variation of wave inundation level is achieved by adjusting the deck level of the topside structure such that the deck is lowered until a prescribed level of inundation in the crest of the wave is achieved. Three different level of wave inundation, 0.4m, 0.7m and 0.9m have been computed with a constant topside porosity of $P = 0.63$ applied on LMA scheme. For the case where beams are represented by a series of screen, $P = 0.63$

is applied to each beam. An averaged porosity of $P = 0.63$ is however, represents the whole topside structure as a sponge component which each MP travel a distance of 1 m before reaching the preceding beam. In the discussion that follows, screen model refers to the load experienced by the beams while the sponge model refers to the load experienced by the main deck structure.

Figure 4.2.1.1, Figure 4.2.1.2, and Figure 4.2.1.3 shows the comparison of WID load between Graaf's and LMA load prediction when screen model of $P = 0.63$ to level of wave inundation of 0.4 m, 0.7 m and 0.9 m respectively. It is observed that in all cases the LMA load prediction are generally lower than the Graaf's load prediction due to the availability of porosity such that it allows more MPs to exit the topside structure with remaining momentum. It appears that the WID load increases when the level of wave inundation increases as supposed. It is due to the increase in number of MPs travel within the topside structure which leads to increase in mass flux and thus WID load.

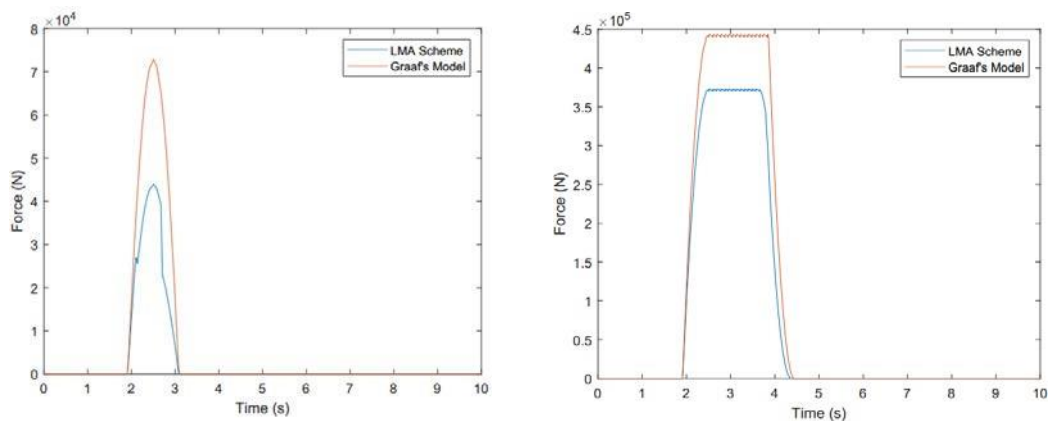


Figure 4.2.1.1. Comparison of Graaf's model and LMA scheme wave-in-deck load prediction on front (left) and bottom (right) deck when screen model of $P = 0.63$ under level of deck inundation at 0.4 m.

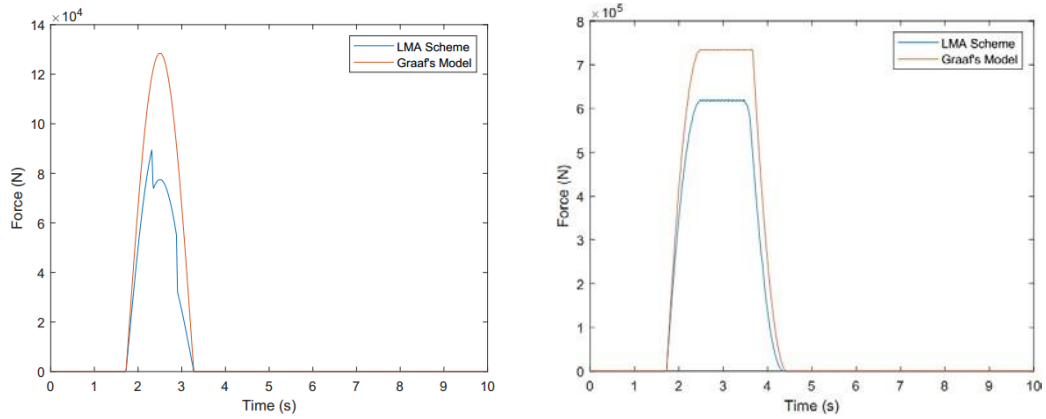


Figure 4.2.1.2. Comparison of Graaf's model and LMA scheme wave-in-deck load prediction on front (left) and bottom (right) deck when screen model of $P = 0.63$ under level of deck inundation at 0.7 m.

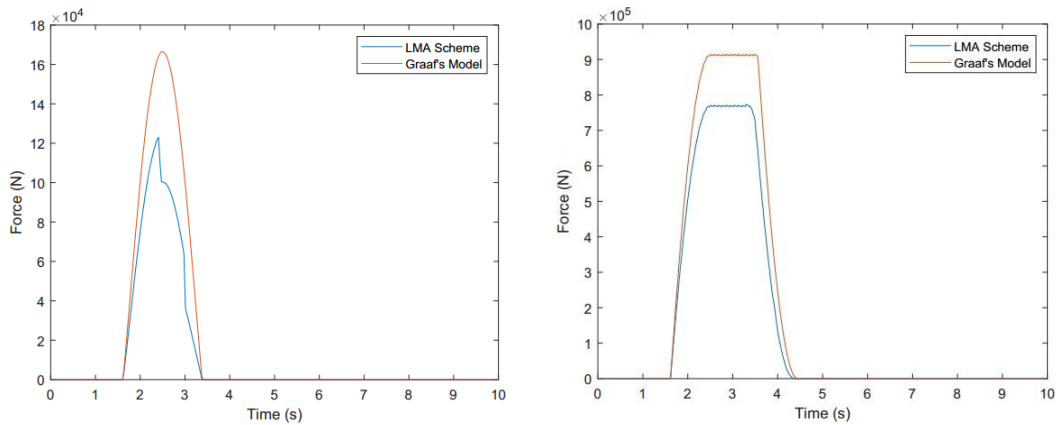


Figure 4.2.1.3. Comparison of Graaf's model and LMA scheme wave-in-deck load prediction on front (left) and bottom (right) deck when screen model of $P = 0.63$ under level of deck inundation at 0.9 m.

Figure 4.2.1.4, Figure 4.1.1.5 and Figure 4.1.1.6 shows the comparison of WID load between Graaf's and LMA load prediction when sponge model of $P = 0.63$ to level of wave inundation of 0.4 m, 0.7 m and 0.9 m respectively. Similar to the screen model, an increase in WID load is found in LMA scheme when level of wave inundation increases, but much lower than the upper bound WID load due to the reason mentioned above.

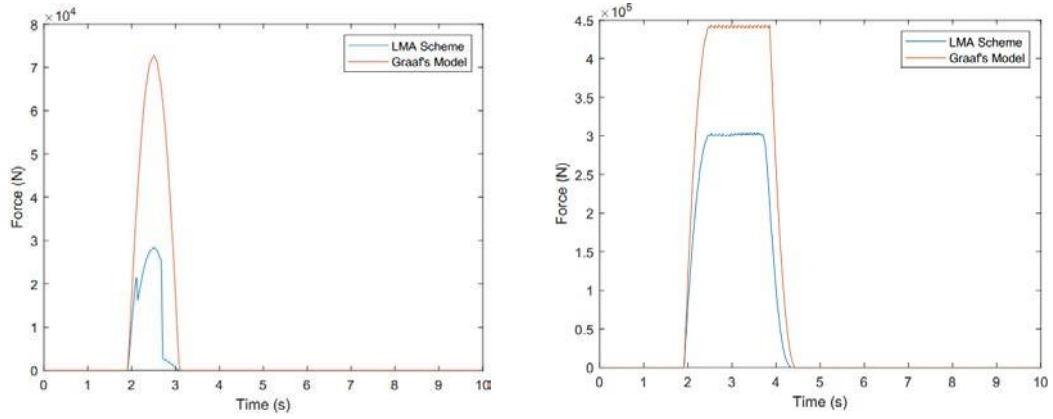


Figure 4.2.1.4. Comparison of Graaf's model and LMA scheme wave-in-deck load prediction on front (left) and bottom (right) deck when sponge model of $P = 0.63$ under level of deck inundation at 0.4 m.

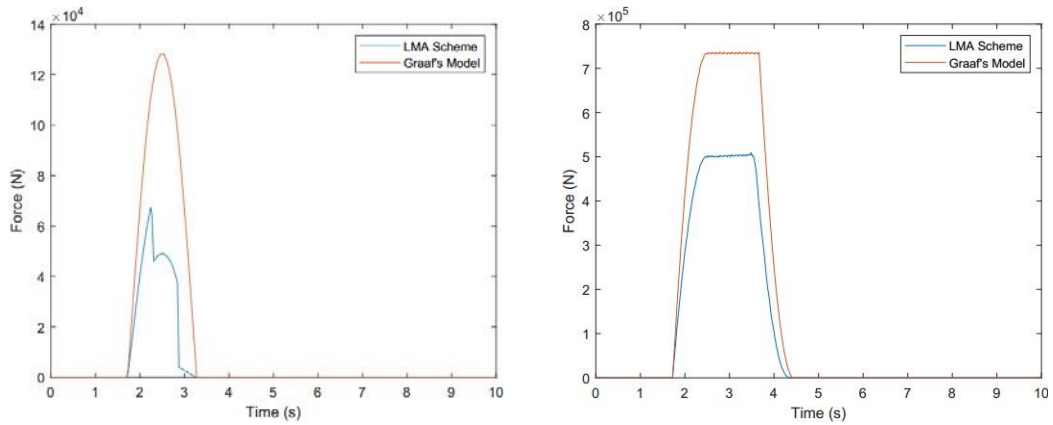


Figure 4.2.1.5. Comparison of Graaf's model and LMA scheme wave-in-deck load prediction on front (left) and bottom (right) deck when sponge model of $P = 0.63$ under level of deck inundation at 0.4 m.

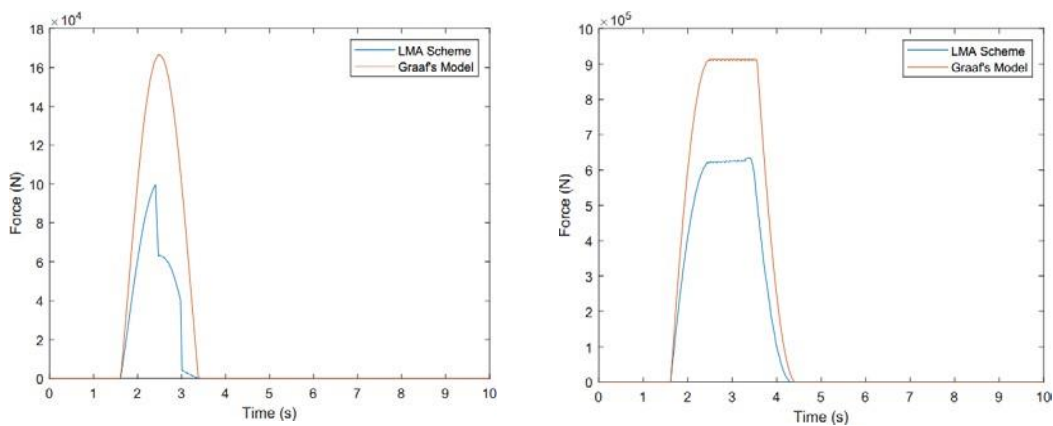


Figure 4.2.1.6. Comparison of Graaf's model and LMA scheme wave-in-deck load prediction on front (left) and bottom (right) deck when sponge model of $P = 0.63$ under level of deck inundation at 0.4 m.

Table 4.2.1.1 below shows the difference in term of percentage of total WID load with respect to Graaf’s model when LMA scheme is applied to both screen and sponge model. The difference given is based on the maximum WID load from summation of both WID loads at front deck and bottom deck. It is observed that overall, the total WID load on screen model is larger than sponge model as momentum is dissipated instantaneously when MPs hit the beam in the former case while the latter allows the MPs to travel a distance before and thus result in gradual dissipation of momentum.

Table 4.2.1.1. Percentage difference of total wave-in-deck load prediction for both screen and sponge model of $P = 0.63$ given different level of wave inundation.

Level of wave inundation (m)	Percentage difference of total WID load prediction (relative to Graaf’s model)	
	Screen model	Sponge model
0.4	-19.2%	-36.0%
0.7	-22.2%	-34.2%
0.9	-18.6%	-34.1%

4.2.2 Variation on topside porosity

This part of the study presents the effect of different topside porosity on WID loads under the same wave condition. Three different porosity (P) in term of open proportion are identified, will be used in LMA scheme. These three values are 0.3, 0.4 and 0.63 respectively. The reason for choosing such values is so that a range of different topside condition are being considered, which P of 0.63 illustrate a rather open topside structure (Ma and Swan, 2020) compared to P of 0.4 and 0.3. For all of the cases the level of wave inundation will be 0.9 m, achieved by adjusting the height of the deck. This would give a same initial MPs and its peak wave particle kinematics.

Similarly, two types of topside structures will be discussed, both screen and sponge model. For screen model, three cases of P each represent the porosity associated within each beam, and same for all other beams while each case were discussed. In contrast, P in sponge model represent the averaged porosity of deck structure as a whole and P proportion of momentum is allowed to pass through after a distance of 1 m travelled.

Figure 4.2.2.1, Figure 4.2.2.2 and Figure 4.2.2.3 shows the comparison of WID load between Graaf's and LMA load prediction when screen model of $P = 0.3$, $P = 0.4$ and $P = 0.63$ with level of wave inundation of 0.9 m applied. Generally, the WID load results from LMA scheme is lower than that of Graaf's, only with different degree. This is due to the accountability of different porosity within the deck in LMA scheme. It can be seen that the WID load in LMA scheme decreases with increasing porosity. Given same initial MPs enter the topside boundary for all cases, each MPs will then carry a P portion of remaining momentum from previous time-step upon passing a screen. Thus, a more porous deck allows more remaining momentum to leave the topside and therefore lesser WID load predicted.

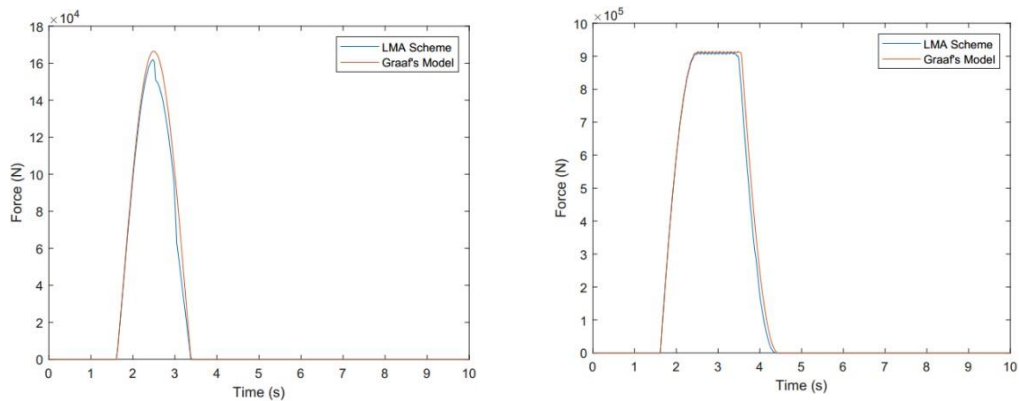


Figure 4.2.2.1. Comparison of Graaf's model and LMA scheme wave-in-deck load prediction on front (left) and bottom (right) deck when screen model of $P = 0.3$ under level of deck inundation at 0.9 m.

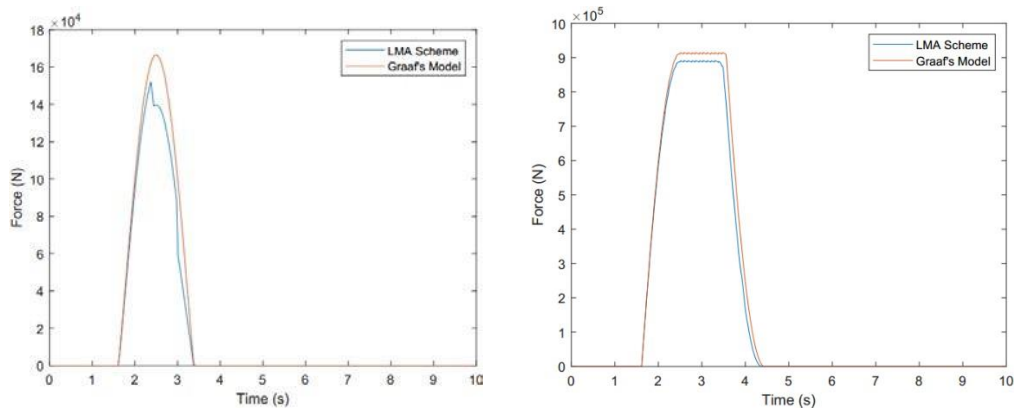


Figure 4.2.2.2. Comparison of Graaf's model and LMA scheme wave-in-deck load prediction on front (left) and bottom (right) deck when screen model of $P = 0.4$ under level of deck inundation at 0.9 m.

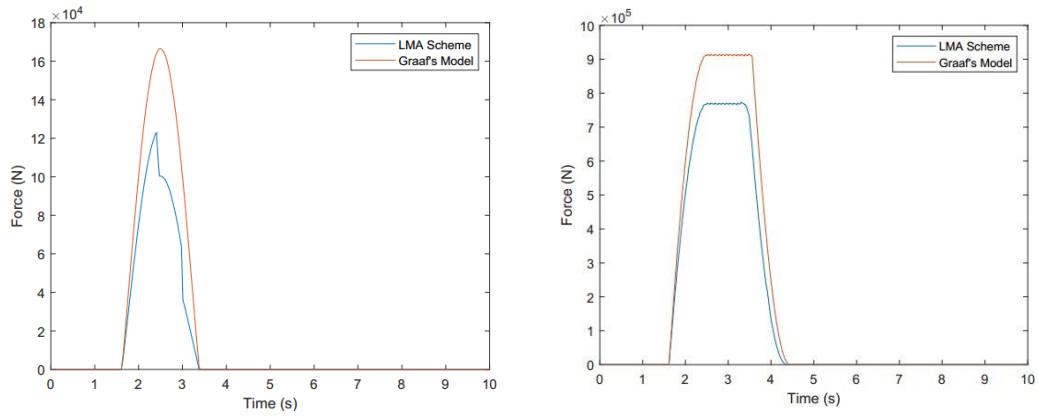


Figure 4.2.2.3. Comparison of Graaf's model and LMA scheme wave-in-deck load prediction on front (left) and bottom (right) deck when screen model of $P = 0.63$ under level of deck inundation at 0.9 m.

Figure 4.2.2.4, Figure 4.2.2.5 and Figure 4.2.2.6 shows the comparison of WID load between Graaf's and LMA load prediction when sponge model of $P = 0.3$, $P = 0.4$ and $P = 0.63$ with level of wave inundation of 0.9 m applied. A similar trend as of screen model can be seen for WID load prediction using LMA scheme due to existence of porosity within the deck.

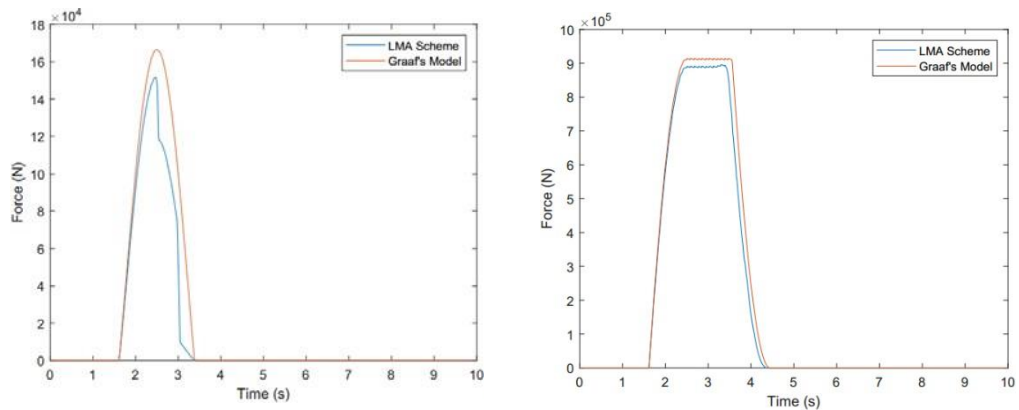


Figure 4.2.2.4. Comparison of Graaf's model and LMA scheme wave-in-deck load prediction on front (left) and bottom (right) deck when sponge model of $P = 0.3$ under level of deck inundation at 0.9 m.

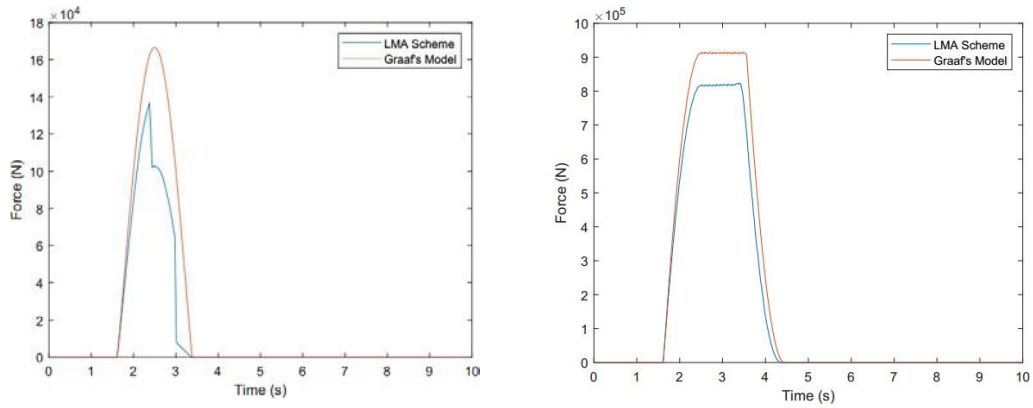


Figure 4.2.2.5. Comparison of Graaf's model and LMA scheme wave-in-deck load prediction on front (left) and bottom (right) deck when sponge model of $P = 0.4$ under level of deck inundation at 0.9 m.

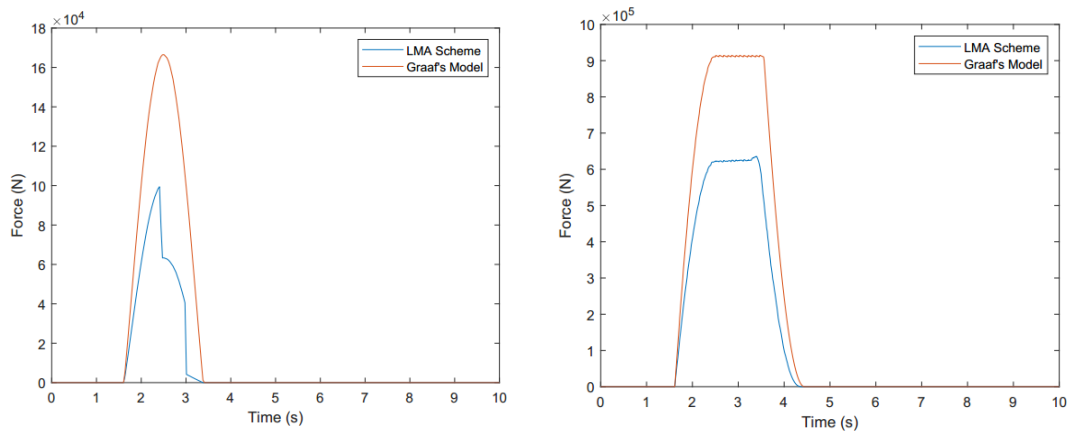


Figure 4.2.2.6. Comparison of Graaf's model and LMA scheme wave-in-deck load prediction on front (left) and bottom (right) deck when sponge model of $P = 0.63$ under level of deck inundation at 0.9 m.

Table 4.2.2.1 shows the below shows the percentage difference of total WID load with respect to Graaf's model when LMA scheme is applied to both screen and sponge model. The difference given is based on the maximum WID load from summation of both WID loads at front deck and bottom deck. However, an instantaneous dissipation of momentum upon hitting the topside features gives a higher WID load prediction in screen model compared to sponge model which allows a gradual dissipation of momentum when MPs travel within the deck.

Table 4.2.2.1. Percentage difference of total wave-in-deck load prediction for both screen and sponge model of level of wave inundation at 0.9 m given different porosity of deck structure

Porosity (P)	Percentage difference of total WID load prediction (relative to Graaf's model)	
	Screen model	Sponge model
0.3	-0.79%	-3.5%
0.4	-3.52%	-12.1%
0.63	-18.6%	-34.1%

4.3 Stokes' 5th order wave

So far the wave kinematics have been computed using linear regular wave theory. As mentioned by Ma and Swan (2020), a crucial factor for the successful prediction of WID using LMA is the use of accurate wave kinematics. Therefore, the more accurate Stokes' 5th order wave theory was also applied as a further study. The same simplified topside model is utilized and had been discussed under Section 4.2. However, the wave case is fitted to act as more near-breaking wave type instead of typical non breaking waves. This is because, the largest spikes in WID loads are associated with breaking waves. This is achieved by computing the WID load given the wave properties such that $\frac{Hk^2}{\omega^2}$ equals to 0.38 approximately, where H is the wave height and k is the wave number. This is so as the wave starts to break when a value of $\frac{Hk^2}{\omega^2}$ is equal to 0.44 and above.

To study this, a higher wave height of 21.2m with level of wave inundation taken as 0.4m is used and will be maintained for both Stokes' 5th order wave and linear wave. This gives a $\frac{Hk^2}{\omega^2}$ value of 0.375, which would be higher than typical non breaking wave case of 0.244 that have been used from the previous section. To better illustrate Stokes' 5th order wave on its WID load produced, a comparison between Stokes' 5th and linear wave is computed on Graaf's model alongside with respective LMA scheme which an example P of 0.63 is given. Figure 4.3.1 and Figure 4.3.2 show the surface wave elevation produced by Stokes' 5th order and linear wave respectively. Given same wave parameters, it can be seen that the steepness of the wave in Stokes' 5th order

is higher than that of the linear wave and same goes to the elevation. This implies that for a given deck height, if Stokes' 5th is used, the level of wave inundation will increase rapidly.

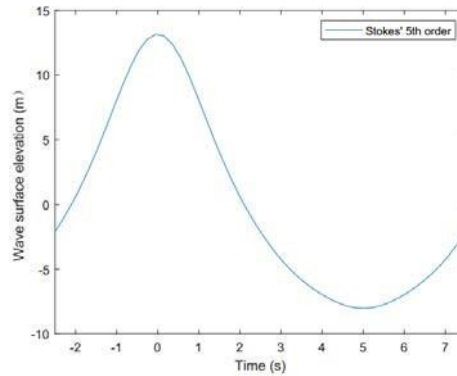


Figure 4.3.1. Surface wave elevation of Stokes' 5th order wave

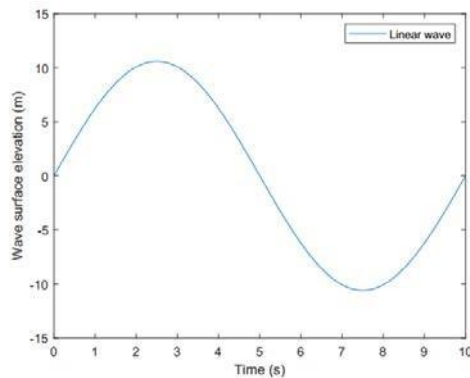


Figure 4.3.2. Surface wave elevation of linear wave

Figure 4.3.3 and Figure 4.3.4 show the WID load computed using Stokes' 5th order wave and linear wave respectively, with each subplot consists of results from Graaf's model and screen model of LMA scheme. It can be seen that the 5th order wave gives higher WID loads compared to linear wave. The reason for this is due to more initial MPs are allow to enter the deck boundary and travel within the deck at a time and thus the total wave kinematics will be larger in Stokes' 5th wave.

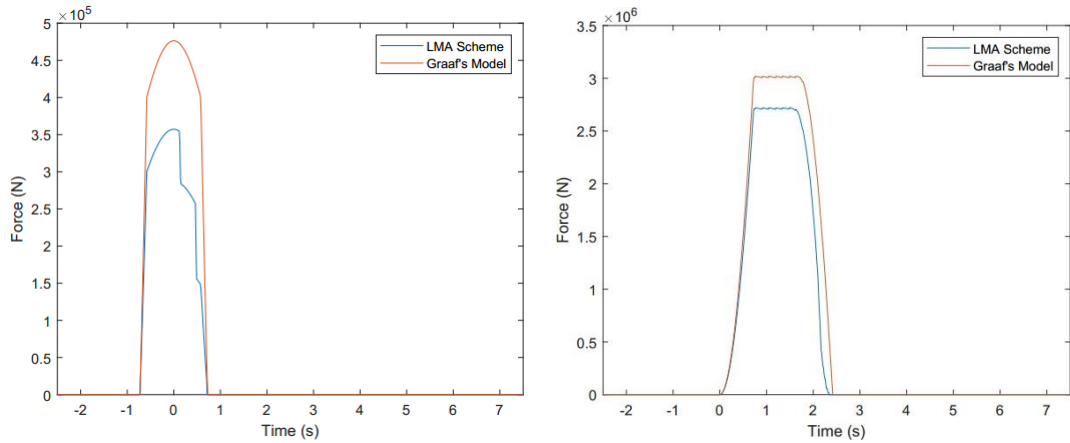


Figure 4.3.3. Stokes' 5th order wave wave-in-deck load prediction on front (left) and bottom (right) deck when screen model of $P = 0.63$ under level of deck inundation at 0.4 m.

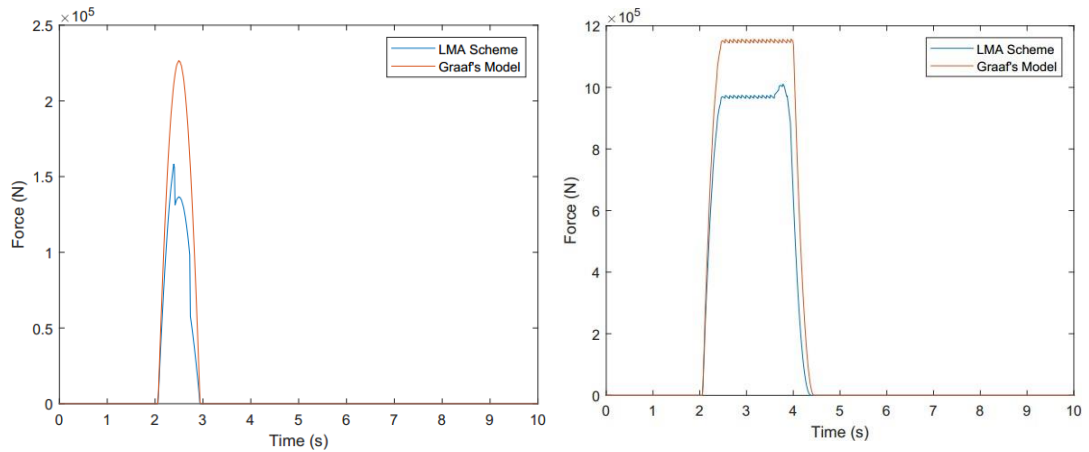


Figure 4.3.4. Linear wave wave-in-deck load prediction on front (left) and bottom (right) deck when screen model of $P = 0.63$ under level of deck inundation at 0.4 m.

Figure 4.3.5 and Figure 4.3.6 show the same comparison but instead sponge model of LMA scheme is used. Same trend on WID load prediction can be seen as of screen model as well. To expect, similar trend will be seen if either porosity or level of wave inundation varied which Stokes' 5th order wave will produce a higher WID loads compared to linear wave.

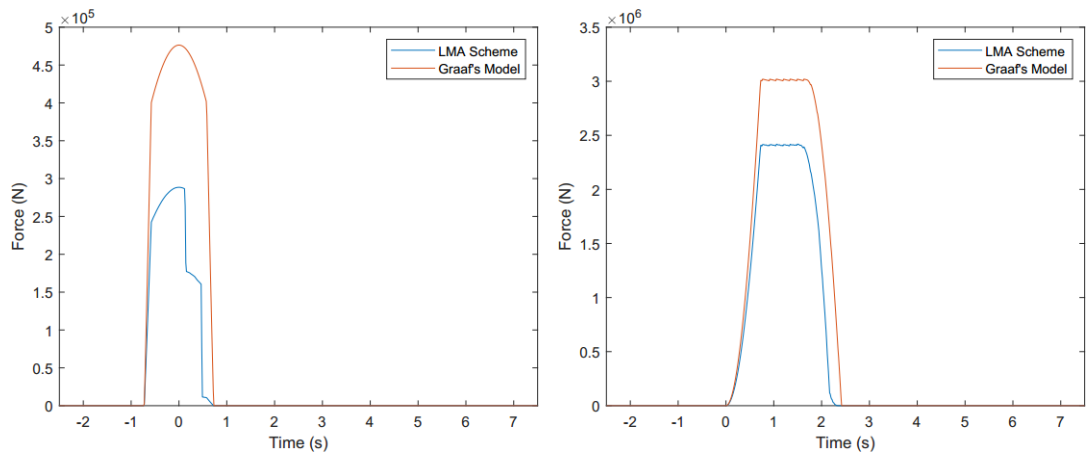


Figure 4.3.5. Stokes' 5th order wave wave-in-deck load prediction on front (left) and bottom (right) deck when sponge model of $P = 0.63$ under level of deck inundation at 0.4 m.

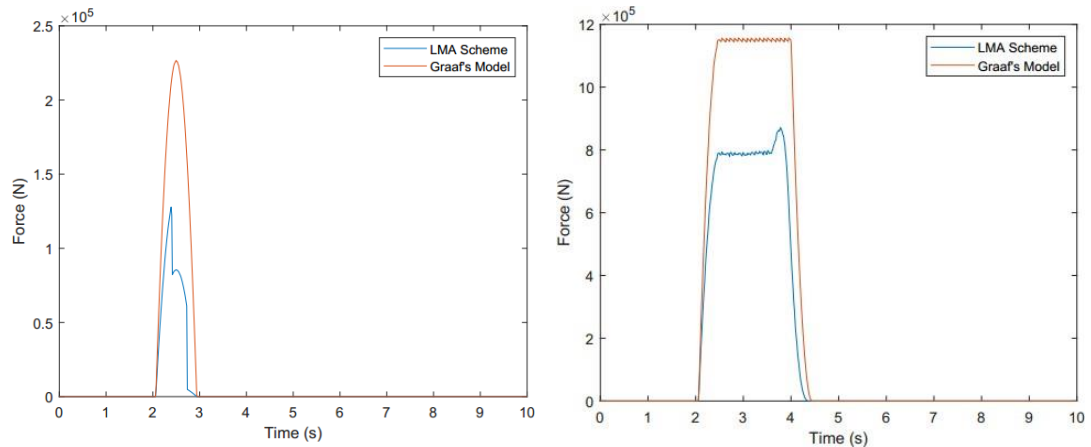


Figure 4.3.6. Stokes' 5th order wave wave-in-deck load prediction on front (left) and bottom (right) deck when sponge model of $P = 0.63$ under level of deck inundation at 0.4 m.

Table 4.3.1 shows the total WID load increases in terms of percentage when Stokes' 5th order wave is applied. It can be seen that when level of wave inundation is at 0.3m, the Stokes' 5th order rises more than half of the linear wave in Graaf's model and undoubtedly a quite similar percentage happened in both screen and sponge model of LMA scheme. In fact, Stokes' 5th order is often adopted to describe wave in real life and such wave gives a greater number of initial MPs to reach at deck boundary and momentum dissipation happens with more MPs pass through the obstruction each time within the deck given same proportion of remaining momentum can be travel until it finally leaves the deck.

Table 4.3.1. Percentage difference of Stokes' 5th order total wave-in-deck load prediction level of wave inundation at 0.3 m and P of 0.63)

		Percentage difference of total WID load prediction (relative to linear wave)
Graaf's model		+60.6%
LMA scheme	Screen model	+63.2%
	Sponge model	+65.9%

It is worth mentioning that only an average of 9 minutes is required to obtain the complete WID load for LMA scheme using a normal laptop. This is important as it has the ability to provide more accurate results by incorporate the topside porosity. In contrast, a CFD computation for the calculation of WID loads typically takes tens of hours (25 hours, according to Ma and Swan (2020)). Given that the code that was used in the present study was not optimized, it is expected that it can run an order of magnitude faster when fully optimized.

CHAPTER 5

CONCLUSION AND RECOMMENDATION

The recently introduced Lagrangian Momentum Scheme (LMA) for the computation of wave-in-deck(WID) load has been implemented in MATLAB in the present study. The code is validated by comparing to the existing simpler model of momentum flux formulation (Graaf et al, 1995) which provides an upper bound solution. A detailed verification process has been undertaken by comparing the force-time history of Graaf's model with LMA scheme. The existence of porosity within the deck brings the total WID loads to be lower than the upper bound prediction. When the deck porosity is set close to 0, the LMA scheme developed in the present study matches Graaf's model closely while a deck porosity of close to 1.0 leads to a force close to 0, as expected. The explanation for this lies in the fact that more remaining momentum are able to exit the deck without dissipation when the deck is more porous and thus proves that the code is indeed able to produce the intended WID load.

The code generated is then applied to a simplified topside structure, represented by a number of screens (for the deck beams) and sponge model (for the main grated deck structure) with typical 100-year wave conditions in South China Sea. The effect of topside and wave parameters on WID load is studied by comparison between Graaf's and LMA scheme. Both screen and sponge models result in a rather consistent decrease in WID load when a relatively open deck structure is adopted, given different level of wave inundations. Higher level of wave inundation which leads to a higher number of MPs entering the deck defines higher overall momentum carried into the deck. Hence the possibility of momentum dissipation when it travels within the deck results in higher WID load. Different porosity in topside structure applied in LMA scheme gives overall lesser WID load compared to Graaf's model, allowed more remaining momentum carried by MPs to leave the deck without obstruction. For a typical porosity of 0.63, LMA scheme predicted the WID load to be reduced up to approximately a percentage of one-fifth in screen model, and up to one-third in sponge model. The

overall reduction of WID load in LMA scheme suggested that porosity would be the dominant parameter when topside features are modelled as sponge due to its ability to allow MPs to travel a distance before momentum dissipate. In contrast, the MPs are brought to rest and momentum dissipated abruptly upon hitting the obstruction in screen model which in this case the dominant parameter would be the level of wave inundation.

Stokes' 5th order wave is later applied to produce a LMA scheme load prediction on nonlinear wave. The nonlinear wave theory which results in an increase in wave steepness and surface elevation also produced a lower WID load compared to upper bound solution, even though it produces a force higher than linear wave.

It is important to note that no empirical coefficient is required while LMA scheme is implemented. Users are able to better represent a more realistic deck structure either by screen or sponge model, to incorporate with possible deck porosity. This in fact, reduced the running time to finally get a more accurate WID load prediction.

The current preliminary study of application of LMA to existing structures can be further enhanced with the following suggestions for further work:

1. Incorporate a more detailed deck representation, ideally, improve the code to import existing CAD drawings of decks. This would allow a detailed structure of the deck to be incorporated and the porosity to be determined more accurately too. This is in contrast to the simple model of the deck constructed in the present study based upon an illustration from a reference.
2. Although realistic waves are irregular in nature, in the present study, only regular waves have been considered. It is recommended that the highly unsteady irregular waves be incorporated in the prediction of WID. The existing code can be used with minor modifications.
3. Inclusion of nonlinearity with Stokes 5th lead to dramatic changes in the magnitude of the WID loads. It is recommended that fully nonlinear wave elevation and kinematics be incorporated in the predictions as well.
4. The impact loading that results from WID loads can lead to significant dynamic amplification of the total base shear and overturning moment of typical jacket structures. It is recommended that the forces predicted by the WID module

developed in the current study be coupled with a finite element model of the whole jacket to compute the full dynamic loads experienced by the structure.

REFERENCES

- Chaplin, J. R., Greated, C A, Flintham, T P and Skyner, D J (1992) *Breaking wave forces on a vertical cylinder* (Offshore Technology Report) London, GB. Health and Safety Executive, 71.
- Chen, Y., Wu, Y., Bahuguni, A., Gullman-Strand, J., Lv, X., Lou, J., & Ren, W. (2018). Directional wave-in-deck loading on offshore structures with porous and plated decks with supporting I-beams. *Coastal Engineering*, 137, 79-91. <https://doi.org/10.1016/j.coastaleng.2018.03.009>
- DNV-GL (2019b). Recommended Practice DNVGL-RP-C205: Environmental Conditions and Environmental Loads. DNV-GL, Norway.
- Fenton, J. D. (1985). A Fifth-Order Stokes Theory for Steady Waves. *Journal of Waterway, Port, Coastal, and Ocean Engineering* 111, 216.
- Graaf, J. W. v. d., Tromans, P. S., Vanderschuren, L. (1995). Wave loads on decks. *Shell Offshore Struct. Eng. Newsl.* (10).
- Hall, T. (2012). Hurricane isaac costs Gulf of Mexico \$500m to \$1bn. Retrieved from <http://www.offshore-technology.com/contractors/maintenance/welaptegamarine/presshurricane-isaac-costs-gulf-of-mexico-500m-to-1bn.html>. (Accessed on 2020-11-29)
- HSE (1998). Review of wave-in-deck load assessment procedures. Technical Report Technical Report OTO 97 073, Health & Safety Executive, United Kingdom.
- ISO (2014). Petroleum and Natural Gas Industries — Fixed Steel Offshore Structures (ISO 19902:2007/Amd.1:2013). International Organization for Standardization (ISO).
- Kaiser, J. B., & Chambers, M. D. (2017). Offshore platforms and mariculture in the US. *Aquaculture Perspective of Multi-Use Sites in the Open Ocean*, 375-391. https://doi.org/10.1007/978-3-319-51159-7_13
- Kaplan, P., Murray, J. J., Yu, W. C. (1995). Theoretical analysis of wave impact forces on platform deck structures. *In: OMAE 1995, 14th International Conference*

on 42 *Offshore Mechanics & Arctic Engineering*, vol. 1, ASME, Copenhagen, Denmark, 189.

- Latheef, M., & Swan, C. (2013). A laboratory study of wave crest statistics and the role of directional spreading. *Proceedings of the Royal Society A: Mathematical, Physical and Engineering Sciences*, 469(2152), 20120696. <https://doi.org/10.1098/rspa.2012.0696>
- Mat Soom, E., Abu Husain, M. K., Mohd Zaki, N. I., Kamal M Nor, M. N., & Najafian, G. (2018). Lifetime extension of ageing offshore structures by global ultimate strength assessment (Gusa). *Malaysian Journal of Civil Engineering*, 30(1). <https://doi.org/10.11113/mjce.v30.174>
- Ma, L., Swan, C. (2019). An experimental study of wave-in-deck loading and its dependence on the properties of the incident waves. *Journal of Fluids and Structures*, 92. <https://doi.org/10.1016/j.jfluidstructs.2019.102784>
- Ma, L., Swan, C. (2020). The effective prediction of wave-in-deck loads. *Journal of Fluids and Structures*, 95. <https://doi.org/10.1016/j.jfluidstructs.2020.102987>
- Morison, J. R., O'Brien, M. P., Johnson, J. W. & Schaaf, S. A. (1950). The force exerted by surface waves on piles. *Journal of Petroleum Technology* 2, 149.
- NORSOK, 2017. N-003 Actions and Action Effects, third ed. Norwegian Technology Standards Institution (NORSOK), Mustads vei 1, NO-0283 Oslo, Norway.
- Paganie, D., 2008. Ike topples old platforms. Retrieved from: <https://www.offshore-mag.com/articles/print/volume-68/issue-10/departments/gulf-of-mexico/gulf-of-mexico.html> (Accessed on 2020-11-26).
- PETRONAS Technical Standards (2012), Design of fixed offshore structures (working stress condition), PTS 34.19.10.30.
- Tromans, Peter & Vanderschuren, Luc. (2018). WAVE LOADS ON OFFSHORE STRUCTURES.
- Twomey, B.G. (2010). Study assesses Asia-Pacific offshore decommissioning costs. *Oil & Gas Journal*, 108, 51-55.
- U.S. Department of Energy, Energy Information Administration, Independent Statistics & Analysis. (2017). *Country Analysis Brief: Malaysia*. Retrieved from <https://www.eia.gov/international/analysis/country/MYS>

U.S. Department of State, 2006. Hurricane katrina: What government is doing.
Retrieved from: <http://www.state.gov/documents/organization/150082.pdf>
(Accessed on 2020-11-26).

APPENDIX

Manual Calculations of Wave Induced Load on Front Deck and Bottom Deck

Table 1: Wave parameter assumptions

Parameter	Value
Wave period, T	8 s
Wave amplitude aa	1 m
Wave frequency, $\omega\omega$	$0.7854 \text{ rad s}^{-1}$
Wave number, kk	0.0629 m^{-1}
Wavelength, λ	100 m
Water depth, d	60 m
Water density, $\rho\rho$	1025 kg m^{-3}
Height of deck, h_d	0.5 m
Size of deck (length x width)	20 m x 15 m

To verify the code for WID loads on front deck, let

$$ll = \frac{\lambda}{2} = 50 \text{ mm}$$

$$h_{dd} = 0 \text{ mm}$$

$$tt = \frac{TT}{4} = 2 \text{ ss}$$

$$dd = 0 \text{ mm}$$

and this is when force on front deck, F_f at its maximum.

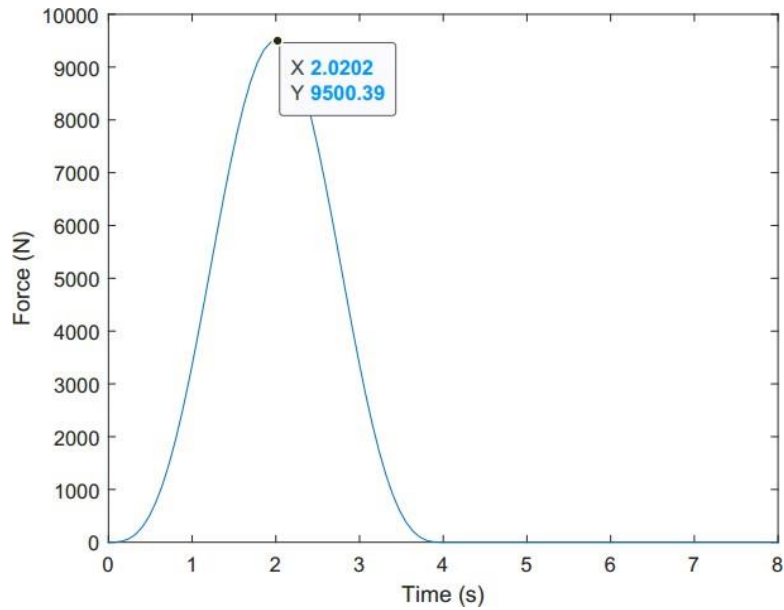


Figure 1: Force computed on front deck using MATLAB for verification

$$u = \frac{a \omega \omega \sin(\omega t - k d)}{h(k d)}$$

$$u = \frac{1 * 0.7854 * \sin(0.0629 * 0 + 0.0629 * 60)}{h(0.0629 * 60)} \sin(0.7854 * 2 - 0.7854 * 0)$$

$$u = 0.7861 \text{ mm/ss}$$

$$\eta = a \sin(\omega t - k d)$$

$$\eta = 1 * \sin(0.7854 * 2 - 0.7854 * 0)$$

$$\eta = 1 \text{ mm}$$

$$F_f = \rho b (\eta - h_{da}) u^2$$

$$F_f = 1025 * 15 * 1 * 0.7861^2$$

$$F_f = 9504.7 \text{ N}$$

To verify the code for WID loads on bottom deck, let

$$L = \frac{\lambda}{2} = 50 \text{ mm}$$

$$h_{da} = 0 \text{ mm}$$

$$t = \frac{T}{2} = 4 \text{ ss}$$

$$d = 0 \text{ mm}$$

and that is when force on bottom deck, F_b at its maximum.

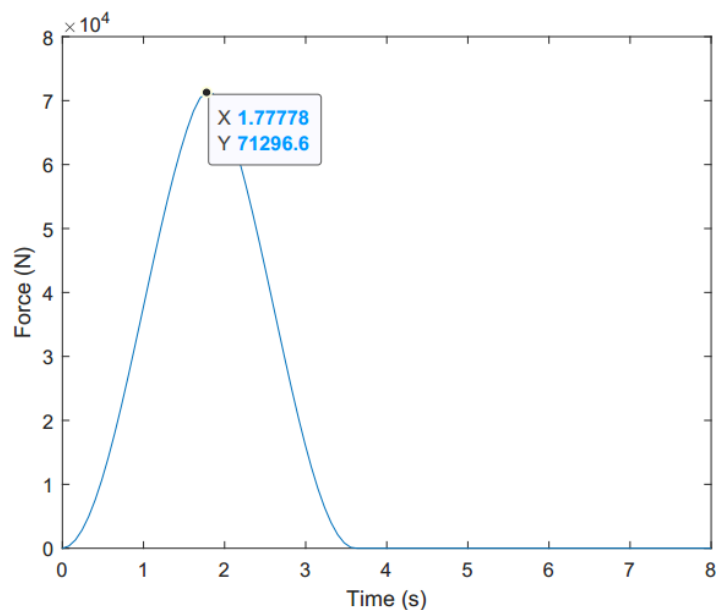


Figure 2: Force computed on bottom deck using MATLAB for verification

$$u = \frac{aa\omega \cosh(kk h_{dd} + kk dd) \sin(\omega t - kk dd)}{1 * 0.7854 * \cosh(0.0629 * 0 + 0.0629 * 60) * \sin(0.7854 * 4 - 0.0629 * dd)}$$

$$\rho = \frac{aa\omega \sinh(kk h_{dd} + kk dd) \cos(\omega t - kk dd)}{1 * 0.7854 * \sinh(0.0629 * 0 + 0.0629 * 60) * \cos(0.7854 * 4 - 0.0629 * dd)}$$

$$F_{bb} = \rho b b \diamond \begin{matrix} xx_{ff} \\ u p p d d d \\ xx_{cc} \end{matrix}$$

$$F_{bb} = 1025 * 15 * 0.7854^2 \diamond \begin{matrix} 50 \\ \sin(3.142 - 0.0629 dd) \cos(3.142 - 0.0629 dd) \\ 0 \end{matrix} d d d d$$

$$F_{bb} = 7.53 dd 10^5 NN$$